Interplay of vitrification and ice formation in a cryoprotectant aqueous solution at low temperature

Christiane Alba-Simionesco, Patrick Judeinstein, Stéphane Longeville, Oriana Osta, Florence Porcher, Frédéric Caupin, Gilles Tarjus

Interplay of vitrification and ice formation in a cryoprotectant aqueous solution at low temperature

Christiane Alba-Simionesco* and Patrick Judeinstein, Stéphane Longeville, Oriana Osta, Florence Porcher
University Paris-Saclay, CEA, CNRS, Laboratoire Léon Brillouin, 91191, Gif-sur-Yvette, France

Frédéric Caupin
Institut Lumière Matière, CNRS, University Claude Bernard-Lyon 1, 6 rue Ada Byron, France

Gilles Tarjus†
LPTMC, CNRS, Sorbonne Université, 4 Place Jussieu, 75005 Paris, France
(Dated: November 24, 2021)

The proneness of water to crystallize is a major obstacle to understanding its putative exotic behavior in the supercooled state. It also represents a strong practical limitation to cryopreservation of biological systems. Adding some concentration of glycerol, which has a cryoprotective effect preventing to some degree water crystallization, has been proposed as a possible way out, provided the concentration is small enough for water to retain some of its bulk character and/or for limiting the damage caused by glycerol on living organisms. Contrary to previous expectations, we show that in the "marginal" glycerol molar concentration $\approx 18\%$, at which vitrification is possible with no crystallization on rapid cooling, water crystallizes upon isothermal annealing even below the calorimetric glass transition of the solution. Through a time-resolved polarized neutron scattering investigation, we extract key parameters, size and shape of the ice crystallites, fraction of water that crystallizes, crystallization time, which are important for cryoprotection, as a function of the annealing temperature. We also characterize the nature of the out-of-equilibrium liquid phases that are present at low temperature, providing more arguments against the presence of an iso-compositional liquid-liquid transition. Finally, we propose a rule-of-thumb to estimate the lower temperature limit below which water crystallization does not occur in aqueous solutions.

PACS numbers:

Significance statement: Studying water crystallization at low temperature and the lower limit of ice formation is crucial both for a fundamental understanding of water and for practical reasons such as cryopreservation. By taking advantage of the polarized neutron scattering technique and by considering a nano-segregated water-glycerol solution we are able to characterize the key parameters of ice formation at temperatures near and below the calorimetric glass transition of the solution and provide a general rule for estimating the lower temperature limit of water crystallization in a broad range of aqueous solutions. We also show that nano-segregated water in the glassy solution at low temperature is not in a high-density form but in a low-density one.

Adding glycerol to water is known to inhibit ice formation because of the perturbation that glycerol produces on the hydrogen-bonding network of water. This property has important consequences both on a practical and on a theoretical level. Glycerol is one example of a cryoprotectant, cryoprotectants being chemicals used to protect biological molecules, organs, plants and insects from freezing[1–9]. Its addition to an aqueous solution may even allow its vitrification, provided a fast enough cooling protocol is applied, thereby opening the possibility of long-term preservation at low temperature of cells, plants, or at a different level protein structures[3], without the damaging interference of ice formation. On the other hand, being able to get around crystallization of water that is otherwise unavoidable in a temperature range between 235 K and around 150 K is a route to study the exciting and actively debated properties of the putative supercooled liquid water in this range[11–13].

In both cases the concentration c_g of glycerol must somehow be optimized. Indeed, a too small concentration is not sufficient to prevent water crystallization by rapid but standard cooling techniques, whereas a too high concentration strongly perturbs water in the mixture which may then lose its resemblance with bulk water; such a high concentration then invalidates the theoretical value of the mixture as a proxy for bulk water and, on the other hand, may damage the living organisms that one is trying to preserve[1,3,5–9]. So, one is especially interested in the lowest glycerol concentration for which glass formation is still possible by rapid cooling, say in liquid nitrogen. It has been shown to be at least 15% in molar concentration[6,8,15,17]. We have then chosen a concentration of about 18% for which, in addition, previously obtained data was available. (Here and in what follows we use the molar concentration c_g; $c_g = 0.18$ then corresponds to a mass concentration of about 52-52.5% depending on the deuteration.)

Our goal is two-fold. First, we want to assess for the "marginal" concentration $c_g \approx 0.18$ at which vitrification is possible with no crystallization upon rapid cooling the factors that characterize water crystallization and deter-

mine the cryoprotective ability of glycerol. The glass state is out of equilibrium and, depending on how deep in it the solution is, it may undergo some form of relaxation and age, which could in rare instances lead to very slow crystallization. Relevant questions that have not been addressed so far are thus: What is the timescale for crystallization in this cryoprotectant aqueous solution at low temperature and how does it vary with temperature? What are the characteristics of ice formation when the solution is in the vicinity of its calorimetric glass transition temperature? Is there a lowest temperature below which ice can no longer appear? Second, we revisit the proposal made by Tanaka and coworkers[5,19] that an "iso-compositional" liquid-liquid transition of the solution, triggered by an underlying liquid-liquid transition of water between a low-density and a high-density phase, takes place for $c_g \approx 0.18$. Although already criticized and, in our opinion, convincingly refuted by several authors[8,15,17], the proposal has been very recently asserted again[20] and it seems timely to add relevant experimental facts to the debate. We thus characterize the liquid phases appearing below melting, emphasizing their out-of-equilibrium character. We show in particular that nano-segregated water in the glassy solution at low temperature is not in a high-density amorphous form but rather in a low-density one.

Our study enables us to describe the stages and the main properties of slow ice formation in a glassy environment. This may be of interest for a better understanding of ice under astrophysical conditions (comets, planets, and interstellar matter)[21]. It also pertains to the broader scope of water polyamorphism and crystallization in electrolytic or nonelectrolytic aqueous solutions, a topic that has been extensively studied (for reviews see, e.g., [22,23]). In particular, based on the temperature dependence of the typical crystallite size that we obtain, we propose a practical way to estimate the limiting temperature below which water crystallization cannot occur for a range of aqueous solutions. The only required piece of information on the solution is its calorimetric glass-transition temperature.

Before any further exposition, it is worth recalling the overall temperature-concentration phase diagram of water-glycerol solutions[2,4–6,8,9,17,25,27,29]: see Fig. S1 in the Supporting Information (SI). It is reasonably well established that below melting, three different ranges of glycerol concentration should be distinguished. At low concentration, $0 < c_g \lesssim 0.15$, the presence of glycerol is not sufficient to prevent crystallization of water even by a deep quench in liquid nitrogen (alternative techniques should then be used: see, *e.g.*, [30]). At high concentration, $0.28 \lesssim c_g < 1$, the cryoprotective effect of glycerol controls the thermodynamic behavior and ice formation is easily avoided by a fast cooling; water molecules are well miscible with glycerol and no significant phase separation takes place. Above the so-called maximally-freeze concentrated solution $c_g \approx 0.38$, it is even virtually impossible to crystallize the solution, no matter how slow the cooling rate, except by introducing a crystal seed[4]. Finally, the intermediate range, $0.15 < c_g \lesssim 0.28$, is the more complex and interesting one, in which a strong dependence on the thermal treatments is found. Water crystallization can be avoided by fast cooling but is then observed upon heating. It is also a range where nano-segregation may play an important role.

The core of our study is a time-resolved structural characterization of the phases and phase transformations of a water-glycerol mixture obtained after a fast quench at low temperature. This is done mostly at the glycerol concentration $c_g = 0.178 \pm 0.005$ through polarized neutron scattering and selective deuterations. An extensive set of data already exists for this concentration or nearby ones[5,6,8,10,14,15,17,25,33], but no detailed structural investigations have been provided so far. Through the time-resolved neutron-scattering experiment we are able to probe the kinetics of phase transformation at constant annealing temperature, which may be very long in the glassy regime (10 hours or more). We further complement our analysis by thermodynamic measurements made by differential scanning calorimetry (DSC) and dynamical measurements obtained by Nuclear Magnetic Resonance (NMR) and Neutron Spin Echo (NSE).

I. RESULTS

Water crystallization near and below the calorimetric glass transition of the "marginal" cryoprotectant solution

Evidence. The glass transition temperature of the fully deuterated aqueous solution with 18% of glycerol is found by DSC (cooling and heating rates of 10 K/min) at $T_g \approx 164.7$ K, *i.e.*, is about 8-10 K above that of the corresponding fully hydrogenated solution: see Fig. S1 of the SI. (Generically, the characteristic temperatures of the deuterated sample are several degrees higher than those of the hydrogenated sample, e.g., about 4 K higher for the melting temperature T_m[7].) We study the evolution of the static structure factor $S(Q)$ of the solution during the annealing at 160 K, *i.e.*, slightly below T_g, and at 170 K, slightly above T_g. Note that due to the fast quench down to 80-90 K ($\sim$ 70-130 K/min) there is no sign of crystallization in the glass phase up to 160 K prior to annealing. (This is discussed in Sec. III of the SI. In addition, in the SI we also provide an account of the effect of changing the cooling protocol on the results.)

We find that water crystallization takes place at 160 K, albeit at a very slow pace. Evidence is shown in Fig. 1 where the isothermal evolution over time of the static structure factor $S(Q)$ of the fully deuterated sample is plotted. The distinctive signatures of ice formation are as follows: (i) a shift of the location of the main peak to a lower wavevector, from $\approx 1.75\mathring{A}^{-1}$ to $1.71\mathring{A}^{-1}$, (ii) a steep increase of the peak with a concomitant narrowing, (iii) an increase at the lowest Q values, and (iv) a strong decrease of the scattering intensity above the main-peak

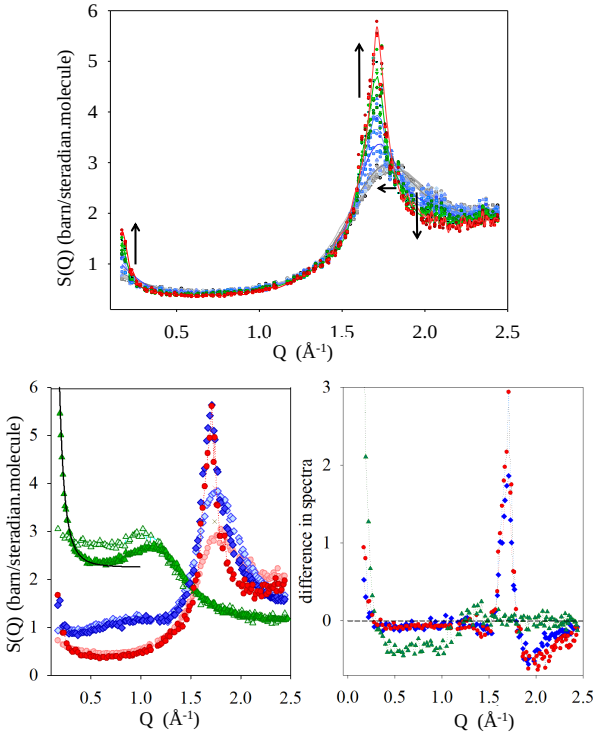

FIG. 1: Top: Evolution of the static structure factor $S(Q)$ of the fully deuterated 17.8% glycerol rich aqueous solution during an isothermal annealing at $T = 160.2$ K, slightly below the calorimetric glass transition $T_g \approx 164.7$ K. Data are colored according to 4 domains of time: gray for 0 to 176 min, then blue up to 366 min, green up to 620 min and finally red up to 721 min. The arrows indicate the main changes with time. Bottom left: Static structure factor $S(Q)$ of the fully deuterated $C_3D_5(OD)_3 + D_2O$ (red symbols) and partially deuterated $C_3D_5(OH)_3 + H_2O$ (green symbols) and $C_3H_5(OD)_3 + D_2O$ (blue symbols) $c_g = 0.178$ solution at the beginning (light color) and the end (dark color) of an isothermal annealing at $T = 160.2$ K; the dark line shows the expected Q^{-4} Porod's law at low Q (an analysis is provided in Sec. VI of the SI). Bottom right: same data shown as a difference between the final and the initial curves.

position, around $2\mathring{A}^{-1}$. This is even more clearly seen by looking at the difference between the data at the beginning and at the end of the annealing that is displayed in the bottom right panel. These features can all be interpreted as resulting from partial crystallization of water: (i)-(ii) the peak at $1.71\mathring{A}^{-1}$ matches the main peak of cubic ice I_c and corresponds to a broadened Bragg peak that grows as more water crystallizes; (iii) the rise at low Q is typical of the formation of interfaces, here between ice crystallites and the remaining liquid phase, and is described by Porod's Q^{-4} law; finally, (iv) the depletion around $2\mathring{A}^{-1}$ is due to a decrease in the spatial correlations between water molecules and the alkyl chains of glycerol resulting from the formation of water crystallites. This decrease already appears when quenching the liquid into the glass due to a nano-segregation leading to the formation of domains of pure water, but it is much more developed when water crystallizes in the domains and more water aggregates to form ice.

To complement this characterization we also display the structure factor $S(Q)$ at the beginning and the end of the annealing for two partially deuterated samples, $C_3D_5(OH)_3 + H_2O$, $C_3H_5(OD)_3 + D_2O$, together with the fully deuterated one, $C_3D_5(OD)_3 + D_2O$. The $S(Q)$ of $C_3D_5(OH)_3 + H_2O$ allows one to focus on the alkyl chains of glycerol, which, as seen from the Figure, tend to become closer as water crystallizes, with a peak in $S(Q)$ moving from about $1.05\mathring{A}^{-1}$ to $1.2\mathring{A}^{-1}$. One can also very clearly see the upswing at small Q's due to the Q^{-4} Porod law associated with the interfaces formed by ice crystallites (see the analysis in Sec. VI of the SI). The structure factor of $C_3H_5(OD)_3 + D_2O$, for which all hydrogen atoms are deuterated except those of the alkyl chains, shows similar features to that of the fully deuterated sample. In particular, the three signatures of water crystallization, namely, the shift, growth and narrowing of the main peak, the upswing at the lowest Q's and the intensity decrease in the region around $2\mathring{A}^{-1}$, can be clearly seen. There are some differences between the curves of this partially deuterated sample and the fully deuterated one: This stems from differences in the prefactors weighting the contributions of the partial structure factors to the total $S(Q)$ obtained by neutron scattering; in particular, the prefactors involving hydrogen atoms are mostly negative, which, because of the overall normalization, mechanically leads to an increase of the prefactors weighting the other contributions.

All of this shows that water crystallization takes place at low temperature just below the glass transition in the presence of a molar concentration of 18% of cryoprotectant glycerol, even after a rapid quench during which no crystallization occurred. This is the main finding of our study, on which we further elaborate below. This crystallization is a consequence of the nano-segregation of the solution that leads to the formation of small domains of water, a phenomenon whose premises can already be found in the liquid structure near the melting temperature[35]. Nano-segregation of water, and its connection to ice formation, is a more general phenomenon that has also been observed for instance in aqueous salt solutions for a range of concentrations[36–38].

We have repeated the analysis for an annealing temperature of 170 K, slightly above the glass transition temperature. We also observe water crystallization, and the evolution is now significantly faster than at 160 K (see below). Water crystallization again appears as a first-order-like transition, as further supported by the presence of an exothermic peak in the DSC measurement: see Sec. VII of the SI. Evidence for water (cold) crystallization at this temperature or at a higher one has already been obtained by previous authors upon heating, by DSC[8,14,17,25], adiabatic calorimetry[6], X-ray scattering[5], dielectric spectroscopy[8], Raman scattering[5,15] and infrared spectroscopy[33].

We note that the $S(Q)$'s obtained by either first an-

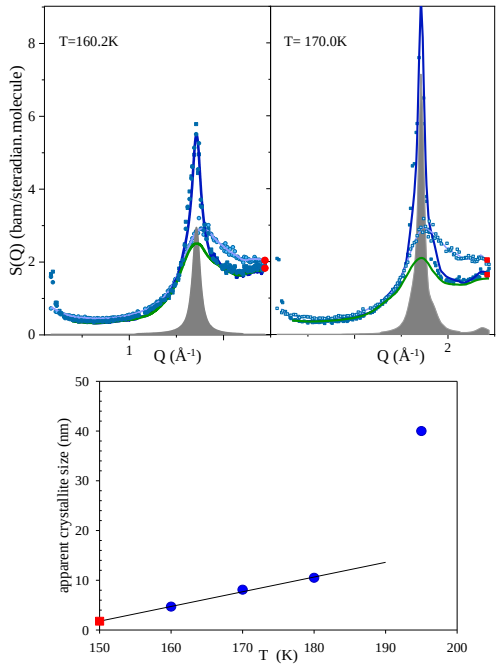

FIG. 2: Top: Rietveld analysis of the structure factor of the fully deuterated sample at $T = 160.2$ K (left) and $T = 170.0$ K (right). In both figures, a light (dark) color indicates the initial (final) $S(Q)$; the dark blue lines correspond to the overall fit, the shaded grey peaks are the resulting crystalline contribution, and the green lines are the remaining amorphous component (cut at low Q to avoid showing the Porod regime). Finally the red points mark the initial and final coherent cross sections at high Q. Bottom: Estimated apparent crystallite size as a function of the annealing temperature. The red square indicates the result of a linear extrapolation of the points at 160, 170, and 180 K down to 150 K.

nealing at 160 K followed by heating at 170 K or annealing directly at 170 K are identical (see Fig. S7 of the SI), a robustness which confirms that metastable states are reached at the end of the annealing times, with no further water crystallization. After heating the sample(s) to still higher temperature and taking measurements at 180 K, 195 K, 210 K and 230 K, we find as expected that water crystallization becomes more and more prominent. In addition, the fraction of hexagonal ice, whose signature can be found in specific peaks of the structure factor, steadily increases: it is negligible within our analysis at 160 K, around 30% at 170 K, 42% at 180 K and almost 62% at 195 K, and 100% at 210 K and above, with no sign of a well-defined transition between I_c and I_h, contrary to what stated in [5]. (Note that the ice that forms at low temperature is generically expected to be a faulty cubic ice with stacks of hexagonal ice, *i.e.*, a "stacking disordered" or "stacking fault" ice,[12,40]; however, the signature of I_h can only be detected in the analysis of the experimentally measured $S(Q)$ when its fraction is large enough and when the crystallites are big enough.)

Crystallite size and ice fraction. Through the analysis of the neutron scattering data we can access some of the characteristics of the ice formed in the transition.

As already described, the peak that grows at 160 K around $1.71\mathring{A}^{-1}$ is a broadened Bragg peak of cubic ice. At 170 K the peak is better resolved and one sees in addition traces of sub-peaks characteristic of hexagonal ice I_h. The broadening of the Bragg peak is of course due to the limited size of the ice crystallites, and from the upper panels of Fig. 2 it is clear that crystallization of water leads to larger crystallites at 170 K than at 160 K. To get an estimate of the typical size we have proceeded to a Rietveld analysis[41] of the data at the end of the annealing process (both for the fully deuterated $C_3D_5(OD)_3 + D_2O$ and the partially deuterated $C_3H_5(OD)_3 + D_2O$ samples, with similar outputs). The procedure is detailed in Sec. Methods and leads to an estimated apparent size of 4.7 ± 0.3 nm at 160 K and of 8 ± 0.5 nm at 170 K. The same analysis gives estimates of 10.5 ± 0.6 nm at 180 K and 40 nm at 195 K: see Fig. 2 (bottom).

Another feature which is potentially crucial for cryopreservation is the fraction of water that crystallizes into ice. One expects (see also [5]) that this fraction increases with the annealing temperature. To estimate the fraction of ice in the solution we focus on the scattered intensity at the high-Q limit of our data, near $2.5\mathring{A}^{-1}$, whose variation reflects the decrease of water content in the solution due to ice formation (see Sec. VIII of the SI). We find that the fraction of water that has crystallized is 21% at 160 K and 39% at 170 K.

Kinetics and timescale. The kinetics of transformation at constant temperature is followed by monitoring several quantities: the maximum of the peak of the structure factor, $S_{\max}$, the intensity at the lowest probed wavevector $Q = 0.19\mathring{A}^{-1}$, $S_{\rm low}$, and the location of the main peak, $Q_{\max}$. The results for $T = 160$ K and 170 K are displayed in Fig. 3. A first observation is that ice formation appears to saturate after some annealing time.

A key feature is the time needed for water crystallization, which can be read from the evolution of $S_{\max}$ and $S_{\rm low}$. At 160 K, crystallization only starts after 100 min and takes around 800 min to be completed, with a typical timescale $\tau_{\rm x} \sim 420$ min. The process is significantly faster at 170 K because crystallization starts after only a few minutes and is completed in less than 100 min with a typical timescale $\tau_{\rm x} \sim 37$ min. By assuming an Arrhenius temperature dependence[42–44], one then obtains an estimate for the typical timescale for crystallization of $\tau_{\rm x} \sim 5400$ min, *i.e.*, almost 4 days, at 150 K.

From the transformation kinetics, we can also analyze the time dependence of the crystallized fraction $\Delta(t)$ through an Avrami fit[45], $\Delta(t)/\Delta(\infty) = 1 - \exp[Kt^n]$ where $K = (1/\tau_{\rm x})^n$ depends on the temperature and on the geometry of the crystal grains and n is the Avrami exponent that is characteristic of the growth mode[46]. By fitting our data, with $\Delta(t)$ obtained from either $S_{\max}$ or $S_{\rm low}$ (see Fig. 3), we obtain $n \approx 2.5 - 2.7$ for $T = 160$ K and $n \approx 2$ for $T = 170$ K. Note that the trend is fully

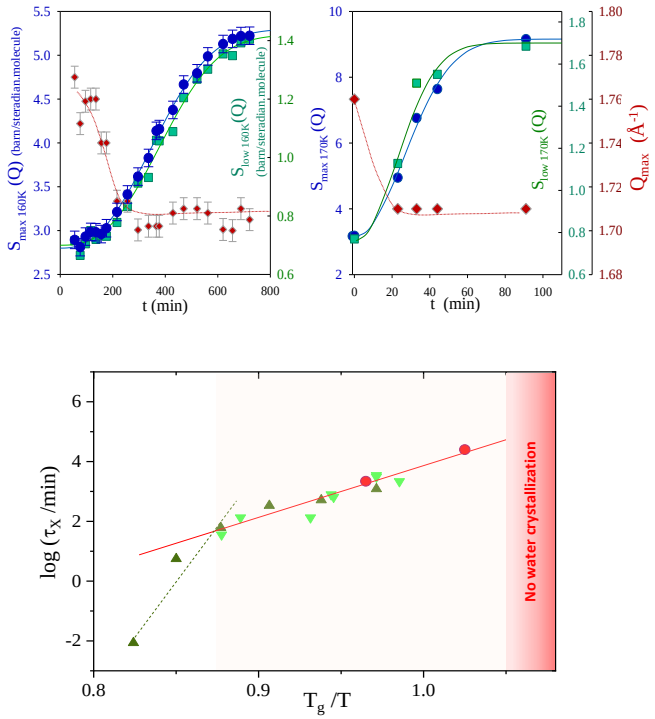

FIG. 3: Top: Crystallization kinetics at $T = 160.2$ K (left) and $T = 170$ K (right). The maximum of the structure factor $S_{\max}$ (blue circles) and the intensity at the lowest measured Q, $S_{\rm low}$ (green squares), are plotted versus time in minutes. The lines are the best fits to an Avrami formula (see the main text). We also display in both cases the evolution with time of the location $Q_{\max}$ of the main peak (red diamonds and right scale). Bottom: $\log_{10}$ of the crystallization time to ice (in seconds) versus T_g/T for the $c_g = 0.178$ water-glycerol solution (red filled circles) and for either hyperquenched[42] (light-green downward pointing triangles) or compressed/decompressed[48] (dark-green upward pointing triangles) pure water at low temperature below 155 K (full red line and associated symbols) where temperature is rescaled by the glass-transition temperature: $T_g = 164.7$ K for the fully deuterated water-glycerol solution and $T_g = 136$ K for pure water. We show for comparison higher temperature data for pure water (dashed green line and associated symbols), which clearly display a distinct behavior[48]. Finally, the red region where no water crystallization takes place is estimated from the minimum crystallite size (see Sec. II).

compatible with the measurement done at $T = 195$ K for the same water-glycerol solution which gives an Avrami exponent of $n \approx 1.7$[33]. The value of n cannot be univocally interpreted, but if one assumes that the nucleation rate is constant and that growth occurs by the diffusion of water molecules toward the existing grains one can conclude that the geometry of the grains is spherical at $T = 160$ K and elongated at $T = 170$ K[46,47]. (The latter is compatible with the more important contribution of ice I_h which tends to grow in a more anisotropic way than I_c.)

Finally, we observe that the evolution of $Q_{\max}$ (see Fig. 3) is quite different than that of the crystallized fraction itself: It is much more rapid at the beginning, where it rather abruptly jumps from ≈ 1.75 to $1.71 \mathring{A}^{-1}$, and then stays essentially constant while growth takes off. This is the manifestation of a first stage in the transformation that consists of nucleation of (faulty) cubic ice. Growth of the grains proceeds when this first stage has been in part completed.

We expect that crystallization is controlled by the diffusion of water molecules as it is for pure water[42–44,49,50]. Below the glass transition of the solution, the glycerol-rich matrix in which nano-segregated water domains are embedded becomes very rigid as temperature further decreases, so that diffusion of water should be closer to that in a nano-confined environment than in pure water and therefore even slower than in the bulk. This effect may be difficult to describe in detail but it is tempting to speculate that it can be accounted at the zeroth-order level through a rescaling of the temperature by the appropriate glass-transition one. Accordingly, we speculate that the dependence on the annealing temperature of the crystallization time to ice at low enough temperature, whether in pure water, water-glycerol solutions, or more generally dilute enough aqueous solutions, is controlled by the dimensionless ratio T/T_g where T_g is the glass transition temperature of the system of interest. (This can only be valid if water is sufficiently nano-segregated in the solution and does indeed crystallize to ice; it is clearly not the case for a homogeneous solution with a high concentration of glycerol, say $c_g \gtrsim 0.28$: see the discussion below.) To test the idea, we have plotted in the lower panel of Fig. 3 our results for the fully deuterated $c_g \approx 0.18$ water-glycerol solution with literature data on pure water at low temperature below ~ 155 K[42,48]. As can be seen from the plot, the rescaling of temperature by T_g indeed provides a very good description. We will discuss the potential benefits of this scaling below.

Evidence against an isocompositional liquid-liquid transition

A point of great fundamental interest raised by the results of Tanaka's group[5,19] is the possibility in a window of glycerol concentration, roughly between 15 and 20%, of an "iso-compositional" liquid-liquid transition triggered by a liquid-liquid transition of water itself between a low-density and a high-density form. Strong arguments have already been given by several groups against this interpretation[8,15,17,23,51], but Tanaka has reiterated his claim in a recent paper[20].

Murata and Tanaka acknowledge that water crystallization comes in the way of the putative liquid-liquid transition but they consider it as an extraneous phenomenon that can be subtracted. They furthermore predict that below a temperature T_L, which is lower than the range they studied, no crystallization should be seen and a pristine liquid-liquid transition could be observed. For

the fully hydrogenated sample with $\sim 18\%$ of glycerol, T_L should be around 162 K, *i.e.*, slightly above the calorimetric glass transition. With the temperature translation discussed above, one then expects a T_L of about 166 K for the fully deuterated sample. Our experiment, done with a rapid quench similar to that used in Ref. [5], is thus safely below the putative T_L when annealing is considered at $T = 160$ K. The outcome, detailed above, is that provided one is patient enough, water crystallization does take place at this temperature and explains the first-order-like transition that is observed. There is no reason to invoke an underlying liquid-liquid transition, and, even less so, an isocompositional one: with the fraction of crystallized water that we have estimated, the glycerol molar fraction of the remaining part of the sample is 21.6% at 160 K and and 24.3% at 170 K instead of the initial composition of 17.8%.

Furthermore, as we discuss below in more detail, the structure of the liquid/glass found immediately after the fast quench and that of the liquid coexisting with ice after partial water crystallization are both dominated by a low-density amorphous (LDA) form of water.

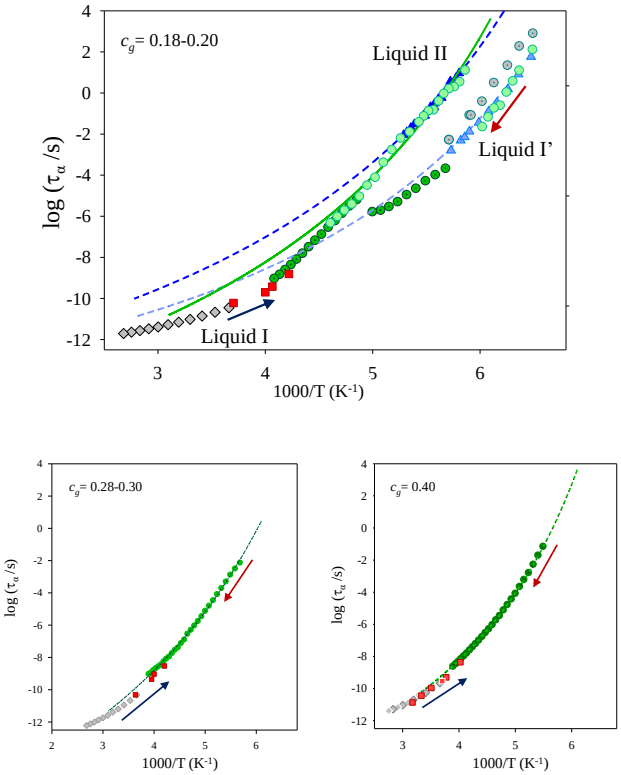

FIG. 4: Arrhenius plot of the relaxation time (in seconds) and the viscosity (rescaled to have an effective time) of the glycerol-water solution for several concentrations: Top: $c_g = 0.18$-0.20; Neutron Spin Echo results ($c_g = 0.178$, red squares) are from the present study, dielectric data are from [8] ($c_g = 0.20$, green circles), [5] ($c_g = 0.18$, blue triangles) and [10] ($c_g = 0.18$, grey circles), and viscosity is from [52] ($c_g = 0.18$, grey diamonds). Dark and light shades correspond to the 2 protocols in [5,8]. The green full line represents dielectric results at $c_g = 0.4$[8] and the dashed lines are fits to the low-temperature dielectric data[5]. Finally, the arrows indicate whether the measurements are performed on cooling or on heating. As detailed in the text, liquid I denotes the stable and weakly supercooled liquid phase, liquid I' the out-of-equilibrium amorphous phase obtained after rapid cooling and prior to ice formation, and liquid II the liquid that remains when ice has formed. Bottom left: $c_g = 0.28$, except for dielectric data ($c_g = 0.30$, green circles)[8]; bottom right: $c_g = 0.40$.

Understanding the liquid phases of the 18% glycerol-water solution in and out of equilibrium

Different liquid phases out of equilibrium. The nature of the liquid phases appearing below melting at a glycerol concentration $c_g \approx 0.18$ is also a vividly debated issue. To list the main proposals: At low temperatures it has been suggested that the system in the glass state or before any significant annealing is a homogeneous solution with water in a high-density amorphous (HDA) form[5,19,20] or a nano-segregated solution[8], possibly with HDA water[17,23]; on the other hand, after heating and/or sufficient annealing, the proposals include a transformation to a homogeneous solution with LDA water (called liquid II[5,19,20]), a phase-separated system with coexistence of ice domains, interfacial water and a water-glycerol liquid mixture close to the maximally-freeze concentrated solution[8,10,17,23], or a supercritical liquid fluctuating between low- and high-density forms of water and prone to crystallization[15]. However, above all, one should stress that the phases observed in this temperature range are out of thermodynamic equilibrium and depend on the thermal treatment. In the following, we distinguish three liquids: *liquid I*, the equilibrium phase above the melting temperature T_m and the continuously related weakly supercooled liquid phase; *liquid I'*, the (out-of-equilibrium) amorphous glass or liquid phase obtained by a fast quench of liquid I and considered prior to any significant annealing; and *"liquid II"*, the (out-of-equilibrium) liquid that remains when the ice that has formed during the annealing is (hypothetically) removed.

Liquid I' versus liquid I. Consider first liquid I'. As already mentioned, there is no sign of ice formation during the fast cooling process. However, except possibly for protocols such as hyperquenches, vapor deposition, or pressure-liquid-cooling vitrification[30] which are not considered here, the liquid nonetheless evolves during the cooling process. Most notably, the nano-segregation which is already detected above melting (see the NMR results in Sec. X of the SI for $c_g = 0.19$ and the computational modeling analysis for $c_g = 0.25$ in [35]) further develops. This can be seen by comparing the structures of liquid I and liquid I' (see Fig. S15 of the SI): the main peak that is typical of water correlations moves from 1.82$\mathring{A}^{-1}$ at 260 K to 1.75$\mathring{A}^{-1}$, grows and sharpens, while there is a drop of the intensity above 2$\mathring{A}^{-1}$ which, as already argued, denotes a decrease of correlation be-

tween water and the alkyl chains of glycerol. (Note that this is even more significant considering that while the main peak shifts to lowers Q's the average density increases from liquid I to liquid I'[3].) This increased nano-segregation is favored by the strong differential in mobility between water and glycerol molecules in the solution. Water becomes increasingly more mobile than glycerol when temperature decreases, as already observed over a limited range of temperature through a NMR study.

The difference between liquid I and liquid I' is also illustrated by looking at their dynamics. To characterize liquid I we have carried out an experimental investigation by neutron spin echo (NSE) in both the stable and the weakly supercooled liquid regimes. Liquid I' has already been studied by broadband dielectric spectroscopy[5,8]. We plot in Fig. 4 the relaxation time obtained from NSE and dielectric measurements, together with viscosity data for liquid I[52], as a function of $1/T$ for $c_g \approx 0.18$-0.20, 0.28, and 0.40. One clearly sees that continuity of the data between liquid I at high temperature and liquid I' at low temperature is only recovered for the highest glycerol concentration shown (in this case the liquid can be supercooled all the way from T_m to T_g). For $c_g \approx 0.18$-0.20 (top panel) the dielectric results also show the abrupt changeover between liquid I' and liquid II resulting from water crystallization, which we discuss below.

The additional hallmark of liquid I', besides being nano-segregated between water domains and a glycerol richer mixture, is that, contrary to what stated or implied before[5,17,19,23,33], there is no trace of water being in an HDA form. To make this clear, we compare in Fig. S14 of the SI the $S(Q)$ that we have obtained prior to any annealing with the neutron scattering curves of LDA and HDA for pure water[15,16]. The main peak of liquid I' is not exactly at the same location as that of the LDA (1.75 versus 1.69-1.71$\mathring{A}^{-1}$), which indicates that the hydrogen-bond network and local tetrahedral order are not as well formed and extended as in the LDA, but there is no resemblance whatsoever with the $S(Q)$ of HDA that peaks at 2.1$\mathring{A}^{-1}$. (The same observation can be made for the X-ray diffraction pattern by comparing the data for liquid I' of [5] with those for HDA and LDA in [55].) Our conclusion is in line with the careful examination of the polarized Raman spectrum by Susuki and Mishima[15], contradicting a previous one by Murata and Tanaka[5], and with the analysis of liquid I at 238 K just above melting by Towey et al.[35]. Note that this conclusion is compatible with the absence of a thermodynamic signature for a first-order transition between LDA and HDA in compression/decompression experiments in the glass[15,17] if one takes into account that the domains of amorphous water are small (of the order of a nm): the transformation from LDA to HDA under pressure is then expected to be very gradual with no clear signature of a transition in thermodynamic measurements.

Nature of "liquid II". A final question is the nature "liquid II". We have shown that water crystallization takes place even below the glass transition, provided one waits long enough, and that ice formation saturates to a given fraction that depends on the annealing temperature (for a given fast-quench protocol). Unfortunately, there is no rigorous way to subtract the contribution of ice from the measured structure factor. If one nonetheless proceeds, as first done in [5] for X-ray scattering, one obtains the curves at 160 K and 170 K displayed in Fig. 2 (upper panels). The remaining structure factor that is obtained after subtraction is distinct from that of liquid I' at the same temperature but the difference is rather subtle: one finds a small shift of the main peak position from $\approx 1.75\mathring{A}^{-1}$ to a value around $1.71\mathring{A}^{-1}$ which roughly corresponds to the peak position of the LDA (see above). Popov et al.[8] have convincingly interpreted their dielectric and DSC data as evidence for what one may call a mesoscopically phase-separated system with water appearing in three different configurations: (i) ice domains, (ii) hydrogen-bonded to glycerol molecules in a more-or-less water-saturated glycerol matrix, and (iii) at the interface between the ice domains and the matrix. It therefore appears plausible that the shift of the main peak to a lower Q observed for the residual structure factor results from an increased contribution of a better tetrahedrally organized interfacial water as well as from the correlations between this interfacial water and the ice. The latter represents a cross-contribution that cannot be removed from the total spectrum, and the structure obtained by subtraction is only a proxy for that of a "liquid II".

If one now considers the evolution of liquid II with increasing temperature, one must account for the fact that more water crystallization takes place. It is then unlikely that the liquid could keep the same composition, be it the original one[5,19,20] or the maximally-freeze concentrated one[8,17,23]. Actually, as seen in the upper panel of Fig. 4 for $c_g \approx 0.18$-0.20, there is a clear signature of the sudden change between liquid I' and liquid II, a change that is a consequence of the partial crystallization of water in the solution. However, upon slow heating, the T-dependence of the dielectric relaxation time of the latter departs more and more from the curve of the 30-40% concentrated mixture to finally meet that of liquid I at high enough temperature. Liquid II is thus an out-of-equilibrium phase, resulting from the transformation of water into ice and whose nature evolves with temperature.

II. DISCUSSION

In addition to a better understanding of the nature of the phases formed out of equilibrium by reheating rapidly quenched water-glycerol solutions and of the interplay between vitrification and ice formation, the present study brings some lessons for cryoprotection. First, we show that, even a few degrees below the calorimetric glass transition, slow water crystallization occurs in an aque-

ous solution with 18% of glycerol; this takes place on a timescale of the order of 10 hours, after which ice formation saturates. Second, we are able to estimate for this solution key parameters that control the potentially damaging effects of ice formation—size and shape of the ice crystallites, fraction of water converted to ice, crystallization time—as a function of the annealing temperature. We find by extrapolating our data that annealing the solution at a still lower temperature, say of 10 K below the lowest one we have studied (160 K in the present case), would lead to a strong increase of the crystallization time that could reach almost 4 days. However, such a time may not be long enough for long-term cryopreservation.

This brings us to take a different angle on the question of the lower temperature limit for water crystallization. Rather than envisaging time as being the limiting factor, one should consider the typical size of the ice crystallites. It has been shown by a combination of experimental and simulation techniques that ice I no longer appears when the ice clusters contain less than 90 molecules at 150 K (and 70 molecules at $\sim$ 100 K)[56]. This corresponds to a size (diameter) of about 1.6-1.7 nm. Using a linear extrapolation of the last 3 data points in Fig. 2 (red line in bottom panel) gives an estimate for the crystallite size of about 1.7 ± 0.1 nm at 150 K. This strongly suggests that ice can no longer form at this temperature.

We now propose to combine this finding with the speculation discussed above that the temperature dependence of water crystallization in dilute aqueous solutions is controlled by the dimensionless ratio T/T_g to provide a rule of thumb for estimating the lowest temperature at which water crystallization can happen in such an aqueous solution: multiply the $\sim$ 150 K estimated here by the ratio of the T_g of the chosen aqueous solution and the T_g of the fully deuterated 18% glycerol-water solution, *i.e.*, 165 K: $T_{\rm lowest}$(solution) $\sim$ (150/165) T_g(solution). Note as a cross-check of the soundness of this relation that it predicts that the lower temperature limit for ice formation in pure water is $\sim$ 124 K, a temperature that seems indeed quite reasonable[15,42,44].

What is the range of aqueous solutions to which this rule-of-thumb may apply? First, although we have focused on cryoprotectant solutions in which organic non-ionic molecules such as glycerol are added to water, electrolytic solutions of water and salt which have been extensively studied are also concerned. Second, the solution should be dilute enough so that water at low temperature is nano-segregated and/or retains some of its bulk characteristics. To get a rough estimate of the upper solute concentration below which this would hold, one could (i) extrapolate the line of homogeneous nucleation of ice and determine when it crosses the glass transition line[3], (ii) locate the crossover concentration at which the (positive) difference between the macroscopic density of the glass and that of the liquid above melting starts to rapidly decrease as concentration further decreases[3], or (i) use structural indicators such that the presence of a rise in the low-Q part of the structure factor below $0.4\mathring{A}^{-1}$ and/or of a shift of the main peak to lower Q's (toward the LDA location) upon quenching the solution to a glass. The usefulness of the latter criterion, which requires that the main peak is sufficiently sensitive to the correlations among water molecules, may depend on the details of the solution: for small solute molecules such as ethylene glycol other contributions involving the solute may be involved, which obscures the behavior of water, and for ionic solutions, one has to take into account the specific organization of water in solvation shells around the ions. For water-glycerol solutions, the above criteria all seem to restrict the range to $c_g \lesssim 0.21 - 0.22$: see Fig. S1 and Sec. I of the SI. For the salt solution of LiCl in water, the upper bound would be a molar concentration of around 12% from criterion (i)[22] and 16% from criterion (ii)[57]. The rule-of-thumb for, say, a 10% solution then predicts that no ice formation is possible below $T_{\rm lowest} \approx (150/165)139 \approx 126$ K. More investigations are certainly necessary to refine the prediction and the range of solutions to which it applies.

As far as cryopreservation is concerned, preventing ice formation is one prerequisite. One should also be able to heat back the sample at room temperature without too much damage caused by ice formation and thawing during the heating process. Considering what we have found in the present study, this seems hard to avoid with a simple glycerol-water solution in the "marginal" concentration range. Other chemicals such as ice recrystallization inhibitors would then be required[58,59]. The knowledge of the crystallites size and shape and of the fraction of ice, as provided in the present study, are then potentially crucial to design the appropriate cryoprotectant mixtures.

III. METHODS

Samples. Thanks to the neutron scattering method, the contribution of partial structure factors can be selectively probed through specific H/D substitutions. The isotopic compositions were chosen in such a way that there was no exchange between H and D during the different thermal treatments nor any uncertainties in the analysis of the scattering data. The sample compositions used for elastic neutron scattering are summarized in Table I of the SI , and detailed below in the sections about DSC and neutron spin echo. The sample concentration c_g is expressed as the number of glycerol molecules divided by the total number of molecules. The samples were purchased from Sigma-Aldrich, Eurisotop and Cambridge Isotope Laboratory and used without any further purification. The deuteration rate is 99.9% for D_2O, 99.9% for fully deuterated glycerol, and above 98% for partly deuterated glycerol.

Polarized Neutron Scattering experiments. The neutron scattering experiments were performed on the D7 spectrometer at the Institut Laue Langevin in Grenoble (France). The main advantage of this instrument

is its ability to separate coherent scattering (containing the structural information) from incoherent scattering by using a technique of longitudinal neutron polarization analysis[60]. The incoherent scattering can be used as an internal calibration. In this way, one directly obtains the coherent scattering signal in absolute units [barn/(steradian.molecule)] and one avoids "vanadium calibration" of the instrument with all its uncertainties. We considered one glycerol concentration, $c_g \approx 0.18$, but several H/D substitutions, with D_2O or H_2O and fully $[C_3D_5(OD)_3]$ or partially deuterated $[C_3H_5(OD)_3$ and $C_3D_5(OH)_3]$ glycerol, were used to independently focus on the contribution of water, of atoms involved in hydrogen-bond network, and of the alkyl chains. We verified for each of the mixtures that the measured $S(Q)$ at high Q in liquid I' prior to any crystallization is fully compatible with the calculated total coherent scattering cross section per steradian and per molecule. The former values were used as a basis to estimate the amount of crystallized water and the glycerol mole fraction of the remaining solution without ice (see Sec. VIII of the SI).

Measurements were performed from 130 K to 300 K in an Orange cryostat by using an alumina annular cell of 0.2 mm thickness and an external diameter of 19.5 mm in order to maximize the transmission. A wavelength of $4.8\mathring{A}$ was chosen to measure the structure factor in the Q-range $0.1\mathring{A}^{-1} < Q < 2.4\mathring{A}^{-1}$. The raw data obtained on D7, *i.e.*, measurements of the non-spin-flip scattered intensity and the spin-flip one, were corrected by using the standard reduction software developed at the ILL (https://www.ill.eu/users/instruments/instruments-list/d7/characteristics). The data are first normalized by the monitor counts. The background, measured from the scattering of the empty cell and a black sample (Cadmium) with the same geometry, was subtracted after taking into account the appropriate self-absorption corrections (*i.e.*, the measured transmission of the sample). The flipping ratio was measured from a quartz rod of the same diameter, and the detectors' efficiency was corrected with a vanadium sample. The incoherent and coherent signals were then calculated from the non-spin-flip and spin-flip scattered intensities. Absorption and multiple scattering were kept negligible by ensuring with a high transmission that only few % of the neutrons were scattered and by choosing cylindrical sample geometry (of only 0.2mm thickness). Thanks to the method, inelastic events included in the incoherent scattering were properly subtracted.

Complementary structural investigations were performed at the Laboratoire Léon Brillouin (LLB) on the instrument G44 (See http://www-llb.cea.fr/fr-en/pdf/g44-llb.pdf) which provides an increased Q-range at the expense of a lower flux and no neutron polarization. Experiments then take longer. A wavelength of $2.89\mathring{A}$ and a cylindrical vanadium cell of 6 mm diameter were used. Results are illustrated for $c_g = 0.28$ in Sec. XI of the SI.

Rietveld analysis. The Rietveld method allows an easy modelling of the peak shape, width and intensity of diffraction patterns in relation with the atomic structure of crystalline phases and their relative contribution[41]. The Rietveld analysis of the polarized neutron scattering data was performed with the FullProf program (see https://www.ill.eu/sites/fullprof/ and [61]). The refinement of the scattered intensities was carried out as a function of the scattering angle 2θ, which is the experimental quantity for a monochromatic diffractometer as D7 (the wave vector Q is then defined as $Q = 4\pi \sin\theta/\lambda$ where the wavelength λ is $4.8\mathring{A}$), by accounting for the instrumental resolution as detailed in [62]. The peak intensity and shape were fitted by taking into account an averaged crystal structure based on the hexagonal I_h and cubic I_c crystalline structures of pure D_2O[63] and their possible combination. The sharpening of the peak with increasing annealing time and/or temperature provides a measure of the average (isotropic) crystallite size. Finally, the difference between the experimental data and the pattern calculated from the structural model corresponds to the averaged residual amorphous part present in the sample. In summary, this analysis gives access to the proportion of hexagonal and cubic ice, to the average size of the crystallites, and to the remaining amorphous or liquid contribution.

Neutron (Resonance) Spin Echo (NSE, NRSE). Neutron spin echo is a powerful quasi-elastic neutron scattering technique to study the dynamical properties of the mixtures in a wide momentum-transfer range and in the range of a few picoseconds to tens of nanoseconds[64]. Neutron spin echo is based on the neutron spin property, *i.e.*, its spin rotation, which encodes the energy transfer occurring during the scattering process. Before and after the process, a magnetic field is applied which generates the precession of the neutron and only depends on the velocity difference of each neutron, irrespective of the initial velocity. As a result, this difference is independent of the chosen wavelength, which means that NSE can use a wide distribution of wavelength while keeping its resolution and boosting the signal intensity. The outcome is the normalized intermediate scattering function $F(Q,t)$; it contains the contributions from both coherent and incoherent functions. However, in a fully deuterated sample the coherent part can be easily extracted, which gives access to the collective component of the correlation function.

The instrument MUSES at the LLB (Saclay, France) combines conventional and Resonance Neutron Spin Echo (NRSE)[65]. The conventional NSE spectrometer is used for measurements at small (so-called Fourier) times ($t < 200$ ps) and the NRSE option gives access to measurements at longer times (200 ps$< t < 2000$ ps). The experiments are carried out with an energy resolution of 0.3 μeV with an incident neutron spectrum of $\delta\lambda/\lambda = 0.15$ bandwidth. We studied fully deuterated samples with several glycerol mole fraction, $c_g = 0.178, 0.28, 0.40$, to cover the whole domain II of the phase diagram in Fig. S1 of the SI. Typical curves are shown in Fig. S11 of the

SI for $c_g = 0.178$ and several temperatures from 200 to 280 K at the wave vector $Q = 1.9\mathring{A}^{-1}$ corresponding to the maximum of the structure factor $S(Q)$ in this range of temperature.

Differential Scanning Calorimetry (DSC). DSC is a thermal analysis that measures the heat flow associated with materials transitions as a function of the time and temperature, in a controlled atmosphere. In the present case, DSC with a cooling rate and a heating rate of 10 K/min was used to determine the temperature of the glass transition of the deuterated samples as well as their melting/freezing phase transitions plotted in Fig. S1 of the SI. No signature of crystallization was observed when cooling at 10 K/min (crystallization only occurred on heating); however, crystallization was observed upon cooling at a rate of 2 K/min. DSC scans are shown in Sec. VII of the SI.

High-resolution and pulsed-field gradient ^{1}H NMR (NMR, PFG-NMR). The NMR sample was prepared with fully protonated glycerol and water at a molar fraction $c_g = 0.19$. The mixture was immediately sealed in a glass tube of 4 mm diameter. NMR spectra were recorded with a Bruker Avance spectrometer at 9.4 T (^{1}H resonance frequency: 400.13 MHz) and a standard dual broadband 5 mm probehead equipped with a gradient coil. A Bruker temperature controller unit using evaporated liquid nitrogen flow allows experiments between 180 K and 330 K with an accuracy and stability of ± 2 K. Temperature calibration was performed with a standard methanol reference tube. Measurement of the area of the different signals gives access to the ratio of mobile and immobile species in the sample, hence to the fraction of crystallized water[66].

Self-diffusion coefficients were measured by PFG-NMR and stimulated echo sequence[67]. The maximum magnitude of the pulsed field gradient was 60 G.cm^{-1}, the diffusion delay Δ was adjusted between 50 ms and 1000 ms, and the gradient pulse length δ was set between 1 ms and 5 ms depending on the diffusion coefficient. The self-diffusion coefficients were determined from the classical Stejskal-Tanner equation[68], $\ln(I/I_0) = -DG^2\gamma^2\delta^2(\Delta - \delta/3)$, where G is the magnitude of the two applied gradient pulses, γ is the gyromagnetic ratio of the nucleus under study, and I and I_0 are the integrated intensities of the signal obtained with and without gradient pulses, respectively. Here, we used 16 equally spaced gradient steps for each experiment. Data acquisition and treatment were performed with the Bruker Topspin software.

Thermal treatments. For the structural studies we quenched the liquid samples in liquid nitrogen from 295 K down to $\sim$ 80-90 K. This roughly corresponds to a cooling rate of 70-130 K/min. The sample temperature was fully stabilized at 90 K and then taken at 130 K at which measurements were performed to characterize the glass phase. The samples were further heated to the chosen annealing temperature close to the glass temperature, *i.e.*, 160 K and 170 K, and we followed the evolution of the structure for long annealing times until the signal was completely stabilized. To give an idea, this took around 13 hours at 160 K. Finally we further heated the sample. We also studied another protocol corresponding to a slow cooling of 3-6 K/min down to the glass at 130 K. We then heated the sample to the temperature at which the measurements were performed: see Sec. IV of the SI.

* Electronic address: christiane.alba-simionesco@cea.fr
† Electronic address: tarjus@lptmc.jussieu.fr

[1] Poldge, C., Smith, A. U., and Parkes, A. S., Revival of spermatozoa after vitrification and dehydration at low temperatures. *Nature* **164**, 666 (1949).
[2] Farrant, J., Mechanism of cell damage during freezing and thawing and its prevention. *Nature* **205**, 1284-1287 (1965).
[3] Fahy, G. M., MacFarlane, D. R., Angell, C. A., and Meryman, H. T., Vitrification as an approach to cryopreservation. *Cryobiology* **21**, 407-426 (1984); Rall, W. F., and Fahy, G. M., Ice-free cryopreservation of mouse embryos at -196°C by vitrification. *Nature* **313**, 573-575 (1985).
[4] Fahy, G. M., Wowk, B., Pagotan, R., Chang, A., Phan, J., Thomson, B., and Phan, L., Physical and biological aspects of renal vitrification. *Organogenesis* **5**, 167-175 (2009).
[5] Zachariassen, K. E. and Kristiansen, E., Ice Nucleation and Antinucleation in Nature. *Cryobiology* **41**, 257-279 (2000).
[6] Fuller, B. J., Cryoprotectants: The essential antifreezes to protect life in the frozen state. *CryoLetters* **25**, 375-388 (2004).
[7] Wisniewski, M., Gusta, L., and Neuner, G., Adaptive mechanisms of freeze avoidance in plants: a brief update. *Environmental and Experimental Botany* **99**, 133-140 (2014).
[8] Stachecki, J.J., Vitrification: Methods Contributing to Successful Cryopreservation Outcomes. In *In Vitro Fertilization* (Eds.: Nagy Z., Varghese, A., Agarwal, A.). (Springer, Cham., 2019).
[9] Fahy, G.M., Wowk, B., Principles of Ice-Free Cryopreservation by Vitrification. In *Cryopreservation and Freeze-Drying Protocols. Methods in Molecular Biology* (Eds.: Wolkers, W.F. and Oldenhof H.), vol. 1257, 21-82 (Springer, New York, 2015).
[10] Shen, C., Julius, E. F., Tyree, T. J., Moreau, D. W., Atakisi, H, and Thorne, R. E., Thermal Contraction of Aqueous Glycerol and Ethylene Glycol Solutions for Optimized Protein Crystal Cryoprotection. *Acta Cryst. D* **72**, 742-752 (2016).
[11] Mishima, O., Calvert, L. D., and Whalley, E., An apparent first-order transition between two amorphous phases of ice induced by pressure. *Nature* **314**, 76-78 (1985). Mishima, O. and Stanley, H. E., The relationship between liquid, supercooled and glassy water. *Nature* **396**, 329-335 (1998).
[12] Poole, P.H., Sciortino, F., Essmann, U., and Stanley, H. E., Phase behaviour of metastable water. *Nature* **360**, 324-328 (1992).

[13] Debenedetti, P. G., Supercooled and glassy water. *J. Phys.: Condens. Matter* **15**, R1669-R1726 (2003).

[14] Inaba, A. and Andersson, O., Multiple glass transitions and two step crystallization for the binary system of water and glycerol. *Thermochimica Acta* **461**, 44-49 (2007).

[15] Suzuki, Y., and Mishima, O., Experimentally Proven Liquid-Liquid Critical Point of Dilute Glycerol-Water Solution at 150 K. *J. Chem. Phys.* **141**, 094505 (2014).

[16] Popov, I, Greenbaum Gutina, A., Sokolov, A. P., and Feldman, Y., The puzzling first-order phase transition in water-glycerol mixtures. *Phys. Chem. Chem. Phys.* **17**, 18063-18071 (2015).

[17] Bachler, J., Fuentes-Landete, V., Jahn, D. A., Wong, J., Giovambattista, N., and Loerting, T., Glass polymorphism in glycerol-water mixtures: II. Experimental studies. *Phys. Chem. Chem. Phys.* **18**, 11058-11068 (2016).

[18] Murata, K. and Tanaka, H., Liquid-liquid transition without macroscopic phase separation in a water-glycerol mixture. *Nature Materials* **11**, 436-443 (2012) and Supplementary Information.

[19] Murata, K. and Tanaka, H., General nature of liquid-liquid transition in aqueous organic solutions. *Nature Com.* **4**, 2844 (2013).

[20] Tanaka, H., Liquid-liquid transition and polyamorphism. *J. Chem. Phys.* **153**, 130901(2020).

[21] Jenniskens, P., and Blake, D. F., Crystallization of amorphous water ice in the solar system. *ApJ* **473**, 1104-1113 (1996).

[22] Angell, C. A., Sare, E. J., Donnella, J., and MacFarlane, D. R., Homogeneous Nucleation and Glass Transition Temperatures in Solutions of Li Salts in D_2O and H_2O. Doubly Unstable Glass Regions. *J. Phys. Chem* **85**, 1461-1464 (1981); Angell, C. A., Liquid Fragility and the Glass Transition in Water and Aqueous Solutions. *Chem. Rev.* **102**, 2627-2650 (2002).

[23] Bachler, J., Handle, P. H., Giovambattista, N. and Loerting, T., Glass polymorphism and liquid-liquid phase transition in aqueous solutions: experiments and computer simulations. *Phys. Chem. Chem. Phys.* **21**, 23238-23268 (2019).

[24] Lane, L., Freezing Points of Glycerol and its Aqueous Solutions. *Ind. Eng. Chem.* **17**, 924 (1925).

[25] Harran, D., Comportement thermique et courbe de transition vitreuse du binaire glycérol-eau. *Bull. Soc. Chim. Fr.* **1-2**, 40-44 (1978).

[26] K. Miyata and H. Kanno, Supercooling behavior of aqueous solutions of alcohols and saccharides. J. Molec. Liq. **119**, 189-193 (2005).

[27] Jensen, M. H., Gainaru, C., Alba-Simionesco, C., Hecksher, T., and Niss, K., Slow rheological mode in glycerol and glycerol-water mixtures. *Phys. Chem. Chem. Phys.* **20**, 1716-1723 (2018).

[28] Nakagawa, H. and T. Oyama, T., Molecular Basis of Water Activity in Glycerol-Water Mixtures. *Front. Chem.* **7**, 731 (2019).

[29] Malfait, B., Pouessel, A., Jani, A., and Morineau, D., Extension and Limits of Cryoscopy for Nanoconfined Solutions. *J. Phys. Chem. Lett.* **11**, 5763-5769 (2020).

[30] Suzuki, Y. and Takeya, S., Slow Crystal Growth of Cubic Ice with Stacking Faults in a Glassy Dilute Glycerol Aqueous Solution. *J. Phys. Chem. Lett.* **11**, 9432-9438 (2020). Suzuki, Y., Non-Segregated Crystalline State of Dilute Glycerol Aqueous Solution. *J. Chem. Phys.* **152**, 144501 (2020).

[31] Hayashi, Y., Puzenko, A., and Feldman, Y., Ice nanocrystals in glycerol-water mixtures. *J. Phys. Chem. B* **109**, 16979-16981 (2005).

[32] Zhao, L.-S., Cao, Z.-X., and Q. Wang, Q., Glass transition of aqueous solutions involving annealing-induced ice recrystallization resolves liquid-liquid transition puzzle of water. *Sci. Rep.* **141**, 15714 (2015).

[33] Bruijn, J. R., van der Loop, T. H., and Woutersen, S., Changing Hydrogen-Bond Structure during an Aqueous Liquid-Liquid Transition Investigated with Time-Resolved and Two-Dimensional Vibrational Spectroscopy. *J. Phys. Chem. Lett.* **7**, 795-799 (2016).

[34] The larger temperature difference for the glass transition, which is 10-12 K for pure water and slowly decreases as c_g increases, stems from quantum effects observed at low temperatures: see Gainaru, C., Agapov, A. L., Fuentes-Landete, V., Amann-Winkel, K., Nelson, H., Köster, K. W., Kolesnikov, A. I., Novikov, V. N., Richert, R., Böhmer, R., Loerting, T., and Sokolov, A. P., Isotope effect in the glass transition of water. *PNAS* **111**, 17402-17407 (2014).

[35] Towey, J. J., Soper, A. K., and Dougan, L. Low-Density Water Structure Observed in a Nanosegregated Cryoprotectant Solution at Low Temperatures from 285 to 238 K. *J. Phys. Chem. B* **120**, 4439-4448 (2016).

[36] Le, L. and Molinero, V., Nanophase Segregation in Supercooled Aqueous Solutions and Their Glasses Driven by the Polyamorphism of Water. *J. Phys Chem A* **115**, 5900-5907 (2011).

[37] Bullock, G. and Molinero, V., Low-density liquid water is the mother of ice: on the relation between mesostructure, thermodynamics and ice crystallization in solutions. *Faraday Discuss.* **167**, 371-388 (2013).

[38] Lane, P. D., Reichenbach, J., Farrell, A. J., Ramakers, L. A. I., Adamczyk, K, Hunt, N. T., and Wynne, K., Experimental observation of nanophase segregation in aqueous salt solutions around the predicted liquid–liquid transition in water. *Phys. Chem. Chem. Phys.* **22**, 9438-9447 (2020).

[39] Hansen,T. C., Koza, M. M., and Kuhs, W. F., Formation and annealing of cubic ice: I. Modelling of stacking faults. *J. Phys.: Condens. Matter* **20**, 285104 (2008).

[40] Moore, E. B. and Molinero, V., Is it cubic? Ice crystallization from deeply supercooled water. *Phys. Chem. Chem. Phys.* **13**, 20008-20016 (2011).

[41] Rietveld, H. M., A profile refinement method for nuclear and magnetic structures. *J.Appl. Crystallogr.* **2**, 65-71 (1969).

[42] Hage, W, Hallbrucker, A., and Mayer, E., Crystallization kinetics of water below 150 K. *J. Chem. Phys.* **100**, 2743-2347 (1994).

[43] Moore, E. B. and Molinero, V., Ice crystallization in water's "no-man's land". *J. Chem. Phys.* **132**, 244504 (2010).

[44] Xu, Y, Petrik, N. G., Smith, R. S., Kay, B. D., and Kimmel, G. A., Growth rate of crystalline ice and the diffusivity of supercooled water from 126 to 262 K. *PNAS* **113**, 14921-14925 (2016).

[45] Avrami, M., Kinetics of phase change. I. *J Chem Phys* **7**, 1103–1112 (1939); Kinetics of phase change. II. *ibid* **8**, 212-224 (1940).

[46] Papon, P., Leblond, J., and Meijer, P. H. E., *The Physics of Phase Transitions: Concepts and Applications.* (Springer, Berlin, 2002).

[47] For the same value of the exponent and still assuming that the growth is diffusion-limited it could also be that the grains are spherical but that the nucleation rate changes

with time. This is not crucial to our analysis.
[48] Lin, C., Smith, J. S., Sinogeikin, S. V., and Shen, G., Experimental evidence of low-density liquid water upon rapid decompression. *PNAS* **115**, 2010-2015 (2018).
[49] Hage, W, Hallbrucker, A., Mayer, E., and Johari, G. P., Kinetics of crystallizing D_2O water near 150 K by Fourier-transform infrared-spectroscopy and a comparison with the corresponding calorimetric studies on H_2O water. *J. Chem. Phys.* **103**, 545-550 (1995).
[50] Scott Smith, R., Huang, C., and Kay, B. D., Evidence for Molecular Translational Diffusion during the Crystallization of Amorphous Solid Water. *J. Phys. Chem. B* **101**, 6123-6126 (1997).
[51] Puzenko, A., Hayashi, Y., Ryabov, Ya. E., Balin, I., Feldman, Y, and Kaatze, U. Relaxation dynamics in glycerol-water mixtures: I. Glycerol-rich mixtures. *J. Phys. Chem. B* **109**, 6031-6035 (2005); Puzenko, A., Hayashi, Y., and Feldman, Y. Space and time scaling in glycerol-water mixtures. *J. Non-Cryst. Solids* **353**, 4518-4522 (2007).
[52] Segur, J. B. and Oberstar, H. E., Viscosity of Glycerol and Its Aqueous Solutions. *Ind. Eng. Chem.* **43**, 2117-2120 (1951).
[53] Koza, M. M., Schober, H., Fischer, H. E., Hansen, T., and Fujara, F., Kinetics of the high- to low-density amorphous water transition. *J. Phys.: Condens. Matter* **15**, 321-332 (2003).
[54] M.-C. Bellissent-Funel, Texeira, J, and Bosio, L., Structure of high-density amorphous water. II. Neutron scattering study. *J. Chem. Phys.* **87**, 2231-2235 (1987).
[55] Urquidi, J., Benmore, C. J., Neuefeind, J., Tomberli, B., Tulk, C. A., Guthrie, M., Egelstaff, P. A., and Klug, D. D., Isotopic quantum effects on the structure of low density amorphous ice. *J. Phys.: Condens. Matter* **15**, 3657-3664 (2003).
[56] Moberg, D. R., Becker, D., Dierking, C. W., Zurheide, F., Bandow, B., Buck, U., Hudait, A., Molinero, V., Paesani, F., and Zeuch, T., The end of ice I. *PNAS* **116**, 24413-24419 (2019).
[57] Elarby-Aouizerat, A., Jal, J.-F., Chieux, P., Letoffé, J. M., Claudy, P., and Dupuy, J., Metastable crystallization products and metastable phase diagram of the glassy and supercooled aqueous ionic solutions of LiCl. *J. Non-Cryst. Solids* **104**, 203-210 (1988).
[58] Davies, P. L., Baardsnes, J., Kuiper, M. J., Walker, V. K., Structure and function of antifreeze proteins. *Philos. Trans. R. Soc. B* **357**, 927-935 (2002).
[59] Budke, C., Dreyer, A., Jaeger, J., Gimpel, K., Berkemeier, T., Bonin, A. S., Nagel, L., Plattner, C., DeVries, A. L., Sewald, N., and Koop, T., Quantitative Efficacy Classification of Ice Recrystallization Inhibition Agents. *Cryst. Growth Des.* **14**, 4285-4294 (2014).
[60] Stewart J. R., Deen, P. P., Andersen, K. H., Schober, H., Barthélémy, J.-F., Hillier, J. M., Murani, A. P., Hayes, T., and Lindenau, B., Disordered materials studied using neutron polarization analysis on the multi-detector spectrometer D7. *J. Appl. Cryst.* **42**, 69-84 (2009).
[61] Rodríguez-Carvajal, J., Neutron Diffraction from Polycrystalline Materials. In *Lecture Notes of the First Summer School on Neutron Scattering*. (Ed.: A. Furrer). (Paul Scherrer Institut Proceedings, Switzerland, 1993), pp 73-95.
[62] Fennell, T., Mangin-Thro, L., Mutka, H., Nilsen, G. J., Wildes, A.R., Wavevector and energy resolution of the polarized diffuse scattering spectrometer D7. *Nuclear Instruments and Methods in Physics Research A* **857**, 24–30 (2017).
[63] Peterson, S. W. and Levy, H. A., A Single-Crystal Neutron Diffraction Study. *Acta Cryst.* **10**, 70-76 (1957). Arnold, J. P., Finch, E. D., Rabideau, S. W., Wenzel, R. G., Neutron-Diffraction Study of Ice Polymorphs. III. Ice Ic. *J. Chem. Phys.* **49**, 4365-4369 (1968).
[64] Mezei, F., Neutron spin-echo–new concept in polarized thermal neutron techniques. *Z. Physik* **255**, 146-160 (1972).
[65] Koeppe, M., Hank, P., Wuttke, J., Petry, W., Gaehler, R., and Kahn, R., Performance and Future of a Neutron Resonance Spin Echo Spectrometer. *J. Neutron Research* **4**, 261-273 (1996). Longeville, S., Neutron spin echo spectrometry with zero field or by resonance. J. Phys. IV France **10**, 59-75 (2000).
[66] Buchtová, N., D'Orlando, A., Judeinstein, P., Chauvet, O., Weiss, P., and Le Bideau, J., Water dynamics in silanized hydroxypropyl methylcellulose based hydrogels designed for tissue engineering. *Carbohydrate Polymers* **202**, 404-408 (2018).
[67] Price, W. S., NMR *Studies of Translational Motion: Principles and Applications.* (Cambridge University Press, 2009).
[68] Stejskal, E. O., and Tanner, J. E., Spin diffusion measurements: Spin echoes in the presence of a time-dependent field gradient. *J. Chem. Phys.* **42**, 288–292 (1965).

Acknowledgments

We thank I. Popov et Y. Feldman for fruitful discussions and access to their dielectric data, A. Wildes who was the local contact on D7 at the ILL, M. Hartmann for discussion on the structural data, F. Legendre for technical support at the LLB (Muses), and M. Bombled for helping on the DSC experiments at the LLB. We also thank the eRMN team of ICMMO (University Paris-Saclay) for providing access to the NMR facility and J. Texeira for useful exchanges and a careful reading of the manuscript.

Author contributions

C. A.-S. and G. T. conceived the research and wrote the manuscript, C. A.-S., G. T., and F. C. performed the neutron scattering experiment on D7 for which C. A.-S. analyzed the data; O. O. carried out the DSC measurements and C. A.-S. analyzed them; F. P. contributed to the diffraction experiments on G44 and to the Rietveld analysis of the structural data; P. J. performed and treated the NMR experiments; S. L., O. O., and C. A.-S. conducted and analyzed the NSE measurements.

Additional information

The authors declare no competing financial interests.

SUPPLEMENTARY INFORMATION

APPENDIX A: TEMPERATURE-CONCENTRATION PHASE DIAGRAM OF WATER-GLYCEROL SOLUTIONS

We show in Fig. 5 the phase diagram of water-glycerol solutions where three different ranges of glycerol concentration can be distinguished below the melting line. The range of prime interest for the present study is that in which water is nano-segregated and is part of region II. In region I, water crystallizes upon even rapid cooling (hyperquenches and alternative techniques may still prevent this to happen, as for pure water) and one can define a line of homogeneous nucleation where micrometer size crystallites of ice are formed when cooling (e.g., by using an emulsification method)[1,2]: the experimental points are displayed as downward pointing (blue) triangles in Fig. 5 and the data can be extrapolated as shown by the dotted blue line. The extrapolation crosses the glass transition line around $c_g \approx 0.21 - 0.22$. This value can tentatively be taken as the upper limit of the region where nano-segregation is possible. We suggest that a signature of nano-segregation of water is when the macroscopic density of the solution increases upon quenching, as in a standard molecular liquid, while the main peak of the structure factor shifts to smaller Q, as is characteristic of bulk water. Unfortunately, we have not covered in detail the range between $c_g = 0.15$ and $c_g = 0.22$. We find that the phenomenon does appear for $c_g \approx 0.18$ but is no longer present for $c_g = 0.28$ (see Sec. XI below). An additional criterion is provided by looking at the (positive) difference in macroscopic density between the glass and the high-temperature liquid above melting: This difference is rather constant at high concentration but starts to rapidly decrease around $c_g \sim 0.21$[3]. More work is nonetheless needed to more precisely specify the domain where nano-segregation takes place after rapid cooling to a glass and to extend the study to other aqueous solutions.

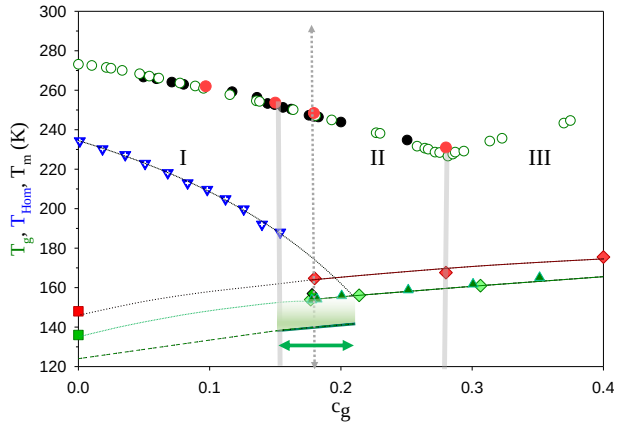

FIG. 5: Phase diagram of the water-glycerol mixture in the temperature versus glycerol (molar) concentration plane. We show the melting line (open[4] and filled[5] black circles) as well as the glass transition line when no crystallization takes place on cooling (dark[5] and light[6] green symbols) for fully hydrogenated samples. The filled red symbols are our results for fully deuterated samples (whose characteristic temperatures are moved up by 3-4 K at melting and 8-10 K at the glass transition[7]). The lines and the extrapolations toward $c_g = 0$ (pure water) are only guides for the eye. As described in the main text, the phenomenology below the melting line is usually divided in 3 regions denoted I, II, and III[8] (see also [9,10]). In region I water crystallization occurs on cooling (even in liquid nitrogen). The intermediate region II, or even a part of it, is the one of interest here, and we mark by a blue vertical dotted line the concentration which we focus on. We also display as downward pointing blue triangles the temperatures of homogeneous nucleation of ice in the solution[1,2] and show as a dotted line a fit and an extrapolation at higher concentrations where it then crosses the glass transition line around $c_g \approx 0.21 - 0.22$. The region between the latter concentration and the boundary of region I ($c_g \approx 0.15$), which is indicated by the large double-headed arrow, is where we expect nano-crystallization of water to take place in the glassy state (obtained after a rapid quench in liquid nitrogen). The full green line in this region is our prediction for the temperature below which ice formation is no longer possible and the extrapolation down to $c_g = 0$ is only indicative.

sample	mass /g	glycerol molar fraction	pseudo-molecule mass/g	σ_{inc} /barn	σ_{coh} /barn	transmission	$\sigma_{coh}/(4\pi)$ /ster.molec
$C_3D_{gC5}(O_gD_{gO})_3D_{w2}O_w$	1.4031	0.178	34.31	6.2942	25.705	0.9	2.046
$C_3H_5(O_gD_{gO})_3D_{w2}O_w$	1.4966	0.178	33.37	76.602	22.392	0.81	1.777
$C_3D_{gC5}(O_gH)_3H_2O_w$	1.4743	0.177	32.05	176.603	17.481	0.67	1.391

TABLE I: Numerical values characterizing the mixtures of glycerol and water for neutron scattering. The sample $C_3H_5(O_gD_{gO})_3D_{w2}O_w$ is only 98% deuterated.

APPENDIX B: DETAILS ON THE CHARACTERISTICS OF THE SAMPLES.

We provide in table I some details on the samples: isotopic composition, glycerol molar fraction c_g, mass of an equivalent molecule, where what is called a "molecule" represents a fictitious molecular unit made of $(1 - c_g)$ molecules of water and c_g molecules of glycerol, incoherent and coherent scattering cross-sections, transmission of the sample on the D7 diffractometer, and finally coherent scattering cross-section per steradian and per molecule.

In Fig. 6 we sketch the molecules of the water/glycerol solutions with their atoms labeled according to Table I.

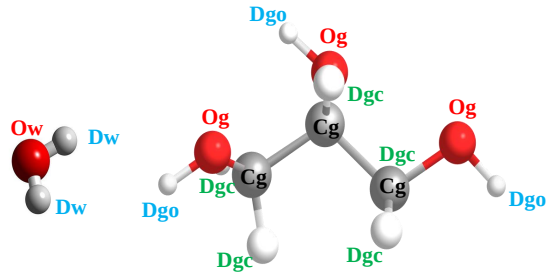

FIG. 6: Sketch of the molecules with their atoms labeled according to Table I.

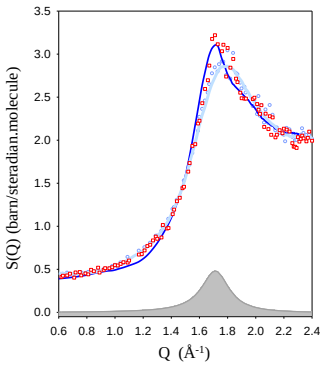

FIG. 7: Structure factor $S(Q)$ of $C_3D_5(OD)_3 + D_2O$ for $c_g = 0.178$ and $T = 160.2$ K obtained by a fast quench in liquid nitrogen. The light blue symbols and the associated interpolating curve correspond to the data prior to any annealing and the red symbols to the data after an annealing of 216min. The dark blue curve is the best Rietveld fit of the data prior to annealing when assuming the presence of ice crystallites of 1.7nm (whose diffraction spectrum is shown by the gray shaded area) on top of an amorphous background. One can see that the agreement is very poor and that the putative system with 1.7nm crystallites rather corresponds to the structure after 216min, where water crystallization has indeed started.

APPENDIX C: ABSENCE OF CRYSTALLIZATION UPON RAPID COOLING.

Evidence that the glassy samples with $c_g \approx 0.18$ obtained through a rapid enough cooling showed no sign of crystallization is as follows:

The structure factor $S(Q)$ after a fast quench in liquid nitrogen and prior to annealing shows no detectable signs of crystallization: the peak is at a $Q \approx 1.75\mathring{A}^{-1}$, somewhat higher than that of ice (and of the LDA), and when we observe crystallization upon isothermal annealing, the first stage is precisely a shift of the peak maximum (see Fig. 3 of the main text); the amplitude of the main peak is also significantly lower than when crystallization proceeds. This can be quantified by resorting to a Rietveld analysis (details on the analysis are given in Sec. Methods of the main text) of the structure factor. Assuming that small ice crystallites of 1.7nm of diameter are present (this is roughly the lower limit size for which ice can form, see Sec. Discussion of the main text) on top of an amorphous background, we look for the best fit to the experimental data. The result is shown in Fig. 7. One can see that the fitted peak is too high and shifted to the left compared to the actual data, even for such a small typical crystallite size. As also displayed in the figure, we find that the reconstructed structure factor with 1.7nm size crystallites rather corresponds to the experimental data after an annealing of 216min, i.e., when crystallization has indeed started in the sample.

A second argument against the presence of ice in rapidly cooled samples comes from the DSC measurements (see Sec. VII below). When cooled at a fast rate of 10 K/min, still slower than the quench in liquid nitrogen that we use for the study of the structure, no sign of crystallization is detected in the DSC scans on cooling. On the other hand, crystallization is observed by using a slower rate of 2 K/min.

Fast enough cooling (10 K/min or faster) therefore seems to completely suppress crystallization for the concentration $c_g \approx 0.18$.

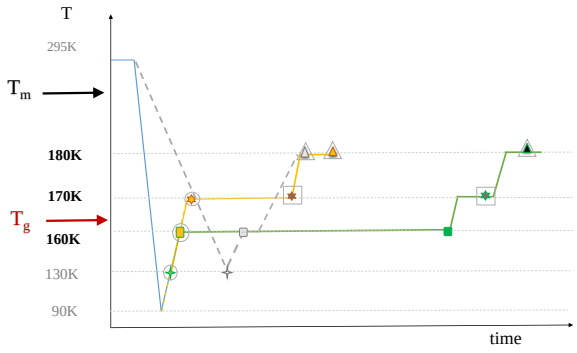

FIG. 8: Sketch of the thermal treatments used in this study. The full blue line and the gray dashed line respectively represent the fast cooling process and the slow cooling one. The symbols indicate some of the points at which structural measurements were taken: The open squares correspond to Fig. 11(left), the triangles to Fig. 11(right), and the circles to Fig. 8 of the main text (liquid I'). The yellow and green horizontal line indicate the annealing stages.

APPENDIX D: INFLUENCE OF THE THERMAL TREATMENT ON THE STRUCTURAL DATA.

For the neutron scattering study we have considered two cooling protocols, the fast quench in liquid nitrogen already discussed and a slow cooling at 3-6 K/min down to 130 K (6 K/min at the beginning, then 3 K/min below 180 K). The slow cooling is followed by heating to

the chosen annealing temperature. The various thermal treatments are sketched in Fig. 8.

The results at 160 K depend on the protocol. We saw that for the fast cooling in liquid nitrogen, crystallization is a slow process taking place over several hours. Alternately, for the slow-cooling protocol, crystallization is much faster. At low temperature, $T = 130$ K, we observe a similar glass structure as for the fast quench, but as soon as one heats the sample, water partly crystallizes: see Fig. 9. Furthermore, whereas we do not detect within our experimental resolution and our analysis hexagonal ice I_h after the fast quench, it appears to form about 16% of the total ice after the slow cooling. Interestingly, the apparent grain size is similar in the two cases ($\sim$ 4-4.5 nm for slow cooling) but the fraction of water that has crystallized is much smaller after a slow cooling: only 7.5% to be compared to the 21% in the other protocol.

On the other hand, when the samples are heated to 180 K, the structure factor is the same, whatever the protocol: see the right panel of Fig. 11 below.

Fig. 9 illustrates two features of cold crystallization in this aqueous solution. First, the structure evolves with increasing temperature from one dominated by features of the cubic ice with a peak around 1.71$\AA^{-1}$ to a mixture of cubic and hexagonal ice and finally to a structure dominated by hexagonal ice with its distinctive triplet of main peaks and an additional peak at 2.38$\AA^{-1}$. The change appears rather gradual, at variance with the suggestion that cubic ice gives way to hexagonal ice as soon as the water grains reach a critical size of about 10-15nm[11]. Second, the dramatic upswing at the lowest probed values of Q which is observed at 180 K is characteristic of interface formation due to many crystallites (as more than 50% of water has crystallized in $\sim$ 10nm grains: see below and main text). At lower temperatures, this effect is less visible because the fraction of ice and the number of grains is smaller. At higher temperatures, the size of the ice crystallites becomes too large for the upswing to appear in our experimental window: the whole Porod behavior moves to lower values of Q to which we did not have access in the D7 experiment.

Finally, in Fig. 10 we compare the structure factor of $C_3D_5(OD)_3 + D_2O$ for $c_g = 0.178$ and $T = 160$ K obtained either by a fast quench in liquid nitrogen (at the end of the isothermal annealing) or by a slow cooling (see also Fig. 9) with that of the stacking disordered ice obtained at 147 K from a different experimental protocol starting from ice V[12]. One can see that there is a clear resemblance in the region of the main peaks between the $S(Q)$ from slow cooling and the stacking disordered ice, the latter being a cubic ice structure disordered by hexagonal stacking faults. There is of course an important amorphous background in the $S(Q)$ of the solution, and the Rietveld analysis that we have performed captures in a crude way this mixture of cubic and hexagonal symmetries. On the other hand, one can check that the $S(Q)$ obtained after a fast quench and prior to any annealing is very different from the two

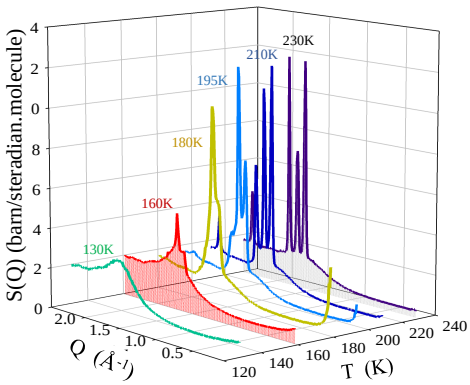

FIG. 9: Structure factor $S(Q)$ of $C_3D_5(OD)_3 + D_2O$ for $c_g = 0.178$ obtained by slow cooling of the sample at 3-6 K/min: it is plotted for increasing temperatures from 130 K to 230 K.

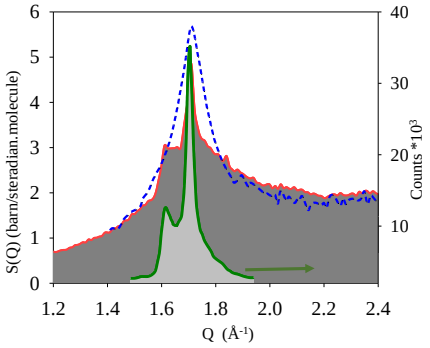

FIG. 10: Comparison of the structure factor $S(Q)$ of $C_3D_5(OD)_3 + D_2O$ for $c_g = 0.178$ and $T = 160.2$ K obtained either by a fast quench in liquid nitrogen at the end of the isothermal annealing (dotted blue line) or a slow cooling (red curve and dark shaded area) with that of the stacking disordered ice obtained from a different protocol and reported in [12] (green curve and light shaded area).

others, in accordance with what already discussed above and in the main text.

APPENDIX E: ROBUSTNESS OF THE STRUCTURE AT 170 AND 180 K VERSUS THE ANNEALING PROTOCOL.

We illustrate here that the states obtained by a fast quench in liquid nitrogen followed by heating and annealing do not depend on the details of the thermal treatment: The structure factors at 170 K are obtained either after a full annealing directly at 170 K or after a full annealing at 160 K followed by heating at 170.3 K; similarly, the structure factors at 180 K are obtained either after a full annealing at 170 K followed by heating at 180.9 K or after a full annealing at 160 K, followed by

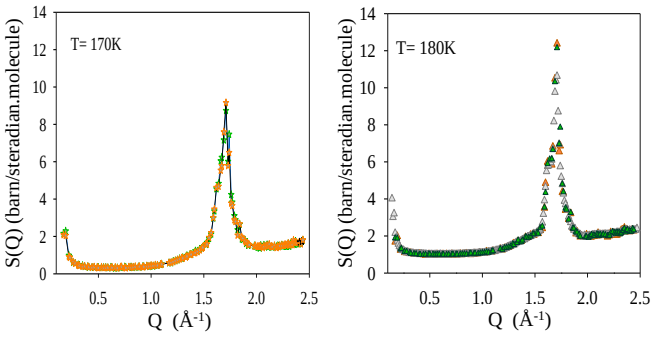

FIG. 11: Structure factor $S(Q)$ of $C_3D_5(OD)_3 + D_2O$ for $c_g = 0.178$ obtained through different thermal treatments. Left, $T = 170$ K: Fast quench in liquid nitrogen, followed by heating and full annealing at 170 K (orange stars); fast quench in liquid nitrogen, followed by heating and full annealing at 160 K, then heating at 170.3 K (green stars). Right, $T = 180$ K: Fast quench in liquid nitrogen, followed by heating and full annealing at 170 K, then heating at 180.9 K (orange triangles); fast quench in liquid nitrogen, followed by heating and full annealing at 160 K, then heating at 170.3 K and finally at 180.6 K (green triangles); in this case we also display the result of the slow cooling in the cryostat to 130 K, then heating at 160 K, and finally at 180 K (gray triangles).

heating at 170.3 K and finally at 180.6 K. The resulting phases with partially crystallized water are very stable (albeit actually only metastable) and no longer evolve with time: this is shown for $T = 170$ K and $T = 180$ K in Fig. 11.

APPENDIX F: ANALYSIS OF THE PREFACTORS OF THE LOW-Q POROD LAW

We consider the amplitude of the Q^{-4} behavior in the low-Q region of the scattered intensity of the fully deuterated and partially deuterated samples after crystallization at 160 K: see Fig. 1 of the main text. Porod's prediction states that in the presence of an interface between two phases the scattered intensity at small wavevectors goes as $I(Q) \sim aQ^{-4}$ with

$$a = 2\pi \left(\frac{S}{V}\right) K^2 \qquad \text{(F1)}$$

where S/V is the area of the interface per unit volume and K^2 is the contrast between the two phases. We then fit our data for each sample at low Q to a functional form $aQ^{-4} + b$ with a and b adjustable parameters. The resulting fits are shown in Fig. 12. As can be seen, the fits are good except for the partly deuterated sample $C_3H_5(OD)_3 + D_2O$ for which the Porod behavior is not well pronounced over the probed range of wavevectors due to the presence of additional contributions near and above $0.3\mathring{A}^{-1}$.

We would like to rationalize the trend observed between the three different deuterations. However, even when looking at the ratios between the amplitudes a, there are still too many unknown parameters. We therefore make some rather crude assumptions to obtain a qualitative or semi-quantitative answer. First, we consider that one of the phase is a mixture of glycerol and water (a proxy for liquid II) with the glycerol concentration $c'_g \approx 0.216$ determined above for the fully deuterated sample (and we take the same value for the other samples) and the other phase is made of ice crystallites. With this assumption, the ratio of the contrasts between two samples denoted 1 and 2 can be obtained as

$$\frac{K_1}{K_2} = \left[\frac{n_{ps}(c'_g)[c'_g(\Sigma b)_{g1} + (1-c'_g)(\Sigma b)_{w1}] - n_w(\Sigma b)_{w1}}{n_{ps}(c'_g)[c'_g(\Sigma b)_{g2} + (1-c'_g)(\Sigma b)_{w2}] - n_w(\Sigma b)_{w2}}\right]^2, \qquad \text{(F2)}$$

where $(\Sigma b)_{g\alpha}$ and $(\Sigma b)_{w\alpha}$, with $\alpha = 1, 2$, are the sums of all coherent scattering lengths for glycerol and water in sample α; n_w is the number density of cubic ice and $n_{ps}(c'_g)$ is the number density of pseudo-molecules comprising c'_g molecules of glycerol and $(1 - c'_g)$ molecules of water. The latter is further approximated by parametrizing the data for the mass density experimentally determined at 77 K in [13] which we divide by the mass of the fully hydrogenated pseudo-molecule at the appropriate concentration: in the range of interest, a quadratic fit to the resulting number density is very good. Finally, we assume that the interface area S/V is roughly the same for the three samples, so that the ratio of amplitudes a_1/a_2 is given by the ratio of contrasts K_1/K_2.

With the above simplifying hypotheses, we obtain a ratio between $C_3D_5(OH)_3 + H_2O$ (green curve in Fig. 12) and $C_3D_5(OD)_3 + D_2O$ (red curve in Fig. 12) of about 3.8 while the corresponding empirically determined one is 3.3; on the other hand, the predicted ratio between $C_3D_5(OH)_3 + H_2O$ (green curve in Fig. 12) and $C_3H_5(OD)_3 + D_2O$ (blue curve in Fig. 12) is 11.4 while the corresponding empirically determined one is 6.4. One can see that there is a semi-quantitative agreement between calculated and observed ratios with a correct prediction of the trend between samples. (As could be anticipated, a much larger discrepancy is found when $C_3H_5(OD)_3 + D_2O$ is involved.) To go further in the analysis and obtain an estimate of a residual glycerol concentration that could account for the potential presence of interfacial water, it would be necessary to carry out systematic experiments with smaller wavevectors by Small-Angle Neutron Scattering.

APPENDIX G: DSC MEASUREMENTS.

We have used two DSC Q-100 from TA instruments, depending on the temperature range explored. One of them was equipped with a compressor and able to go down to 193 K, and the other was equipped with a liquid

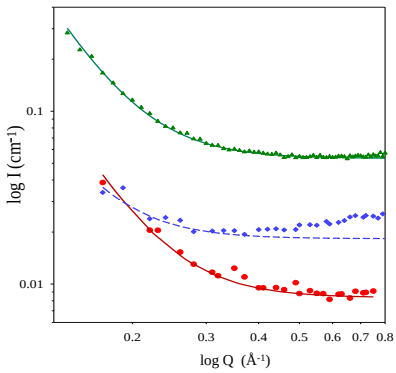

FIG. 12: Log-log plot of the scattered intensity at low Q for the three different deuterations of the glycerol-water solution with $c_g = 0.178$ at 160 K at the end of the annealing when water has crystallized: same data and color code as in Fig. 1 of the main text. The lines are the best fits to Porod's law, $I(Q) = aQ^{-4} + b$. The fit to the $C_3H_5(OD)_3 + D_2O$ data (dashed blue line and symbols) is only indicative as over the range of probed wavevectors the Porod regime does not emerge distinctly enough.

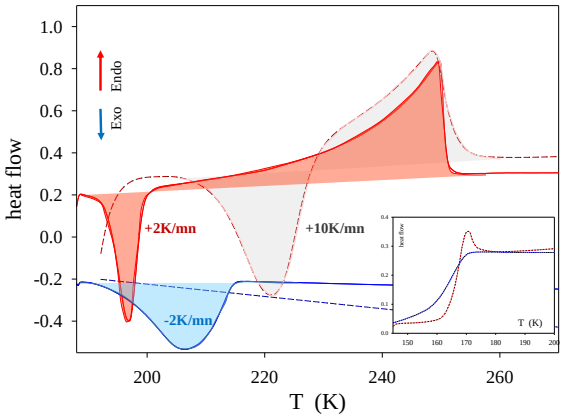

FIG. 13: DSC scans of a fully deuterated sample $C_3D_5(OD)_3 + D_2O$ for $c_g = 0.179$ upon cooling (in blue) and heating (in red). The dashed lines are for a rate of 10 K/min and the full lines of 2 K/min. The areas under the crystallization and the melting peaks correspond to the latent heat exchanged during the process. The scans have been rescaled in the figure. Inset: glass transition of the fully deuterated sample with cooling/heating rates of 10 K/min.

nitrogen cooling system and able to reach temperatures as low as 140 K.

Two distinct cooling/heating rates have been applied on a fully deuterated sample with glycerol molar fraction of $c_g = 0.179$: see the representative scans in Fig. 13. At 10 K/min crystallization is only observed on heating and is immediately followed by melting. From the heat exchanged, one can estimate that 26.4% of water crystallizes, while the remaining water is kept trapped in the glycerol matrix (or at the interface with ice crystallites) with an estimated glycerol molar fraction of then 22.7%. After melting, the melted water is redissolved in the mixture. At 2 K/min, we observe crystallization already on cooling. It is also found on heating, at much lower temperatures than for the faster rate. On cooling, 20% of water crystallizes which leads to a remaining solution with a mole fraction $c_g \approx 21.3\%$ (and consequently to a glass transition at a molar fraction distinct from the original composition). On heating, an additional 12.7% of water crystallizes, an amount that could be considered as representing "free or interfacial water" after the glass transition. The remaining glycerol/water liquid mixture contains $\sim 23.1\%$ of glycerol. Note that the spread of melting is much larger, almost over 50 K, for the slower protocol and the maximum of melting occurs at a slightly larger temperature. Both aspects illustrate the larger crystallites and wider distribution of crystallite sizes when the kinetics is slow (higher T_m). The above results are fully compatible with previous ones obtained in [8,14].

The procedures are different than those applied during the structural measurements (see above and main text) and crystallization takes place in different temperature ranges. However, the trends shown by the two sets of measurements fully agree. We always observe water (cold) crystallization upon heating but crystallization on cooling depend on the cooling rate: no water crystallization for fast enough cooling (10 K/min in DSC and down to 3-6 K/min in structural measurements) but crystallization for a slower rate of 2 K/min (DSC).

APPENDIX H: ESTIMATE OF THE ICE FRACTION FROM THE HIGH-Q SCATTERED INTENSITY.

For a molecular liquid, the static structure factor $S(Q)$ is obtained from the relative positions of the atoms in the sample as the sum of an intramolecular form factor, $F(Q)$, and an intermolecular contribution, $D_m(Q)$. $D_m(Q)$ is the sum of all the interatomic components for atoms belonging to distinct molecules and its Fourier transform gives the intermolecular pair correlation function. The form factor $F(Q)$ can be calculated from the geometry of the molecules: it is the sum of all the pair correlations between atoms of the same molecule. At large Q, *i.e.*, small distances, only the signature of the molecular form factor prevails in $S(Q)$: this is illustrated in Fig. 14 for pure water[15,16] and pure glycerol[17], where one can see that above $2.4\mathring{A}^{-1}$ the form factor dominates $S(Q)$ for both liquids. Similarly, for the mixtures of the present study, the value of the measured coherent differential scattering cross section around $2.4\mathring{A}^{-1}$ only depends on information at the molecular scale. The experimental data around $2.4\mathring{A}^{-1}$ (see Fig. 2 of the main text) corresponds to the coherent differential scattering

cross section in absolute units (barn per steradian and per molecule), which we verify to be equal, before water crystallization takes place, to the calculated value listed in Table I within an uncertainty of 0.5%. For each of the two annealing temperatures shown in the upper panels of Fig. 2 (main text), the two red points at $2.4\mathring{A}^{-1}$ correspond to the signal of the mixture initially prepared at $c_g = 0.178$ before water crystallization (highest point) and to the mixture after partial crystallization of water (lowest point). As a result of ice formation, the latter signal contains less water molecules and accordingly a higher glycerol molar fraction c'_g. The pseudo-molecule used to compute the coherent differential scattering cross section from the data in Table I is thus made of of $[(1-c_g)$ molecule of water + c_g molecule of glycerol] for the initial signal and of $[(1-c'_g)$ molecule of water + c'_g molecule of glycerol] for the final one. The difference between the two measured data points at $Q = 2.4\mathring{A}^{-1}$ then gives access to the amount of water that crystallizes and to the average glycerol molar fraction of the remaining uncrystallized mixture.

At 160 K, before any annealing, the initial value $\sigma_{\mathrm{coh,init}}/(4\pi)$ at $2.4\mathring{A}^{-1}$ is 2.045 barn/(steradian.molecule) with $c_g = 0.178$. At the end of the crystallization process, the final value $\sigma_{\mathrm{coh,final}}/(4\pi)$ is 1.832 barn/(steradian.molecule). This lower value is due to the decrease of the amount of water molecules in the remaining mixture. The proportion of water in the latter is equal to $X_{w,\mathrm{final}} = (\sigma_{\mathrm{coh,final}} - c_g\,\sigma_{\mathrm{coh},g})/\sigma_{\mathrm{coh},w}$, while the initial proportion is simply $X_{w,\mathrm{init}} = (1 - c_g)$ (where w and g refer to water and glycerol, respectively). The fraction of water that crystallizes is therefore $(X_{w,\mathrm{init}} - X_{w,\mathrm{final}})/X_{w,\mathrm{init}}$. At 160 K, 21.3% of water crystallizes, and the remaining mixture has a glycerol concentration $c'_g = 0.216$. There are several sources of uncertainties in this estimation. One may come from the uncertainty on the effective deuteration rate of the sample (a 1% difference in the deuteration of glycerol from 99% to 98% leads to an error of 0.5% in the estimated fraction of crystallized water). Additional uncertainties can be estimated from the small difference between the $Q = 2.4\mathring{A}^{-1}$ value in full structure factor at the end of the annealing and that in the amorphous contribution obtained after removing the crystalline component determined through the Rietveld analysis (green curve in Fig. 2 of the main text): this difference however represents less than 1%, which means a 1% uncertainty in the fraction of crystallized water (22.5% instead of 21.3).

With the second thermal treatment corresponding to the slow cooling protocol, crystallization appears rapidly when the sample is heated from the glass to 160 K, and we find that a fraction of 7.5% of water crystallizes. For the partly deuterated sample $C_3H_5(OD)_3 + D_2O$ shown in Fig. 1 of the main text, the proportion of water that has crystallized is 19.6% with a glycerol mole fraction of $c'_g = 0.212$ in the remaining mixture.

At 170 K, a similar analysis provides $\sigma_{\mathrm{coh,init}}/(4\pi) \approx$ 2.043 barn/(steradian.molecule) with $c_g = 0.178$ and $\sigma_{\mathrm{coh,final}}/(4\pi) \approx 1.641$ barn/(steradian.molecule), from which we extract that $39 \pm 1\%$ of of water has crystallized with a glycerol mole fraction of $c'_g = 0.26$ in the remaining mixture. Finally, at 180 K, 53% of water crystallizes and the glycerol mole fraction in the remaining mixture is $c'_g = 0.32$, not far from the concentration estimated from dielectric measurements by Popov *et al.*[8] for liquid II, *i.e.*, 0.38-0.40.

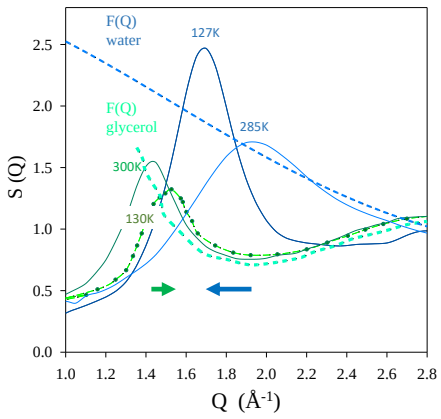

FIG. 14: Static structure factor of bulk water at 285 K (full dark blue line) and at 127 K in the LDA form (full light blue line)[15,16] and of bulk glycerol[17] at 300 K (full dark green line) and at 130 K (full light green line and symbols). The shift of the peak of the $S(Q)$ of water to lower Q's (blue arrow) is related to the density decrease of water as T decreases. In contrast, glycerol behaves as a standard molecular liquid with a shift to higher Q's (green arrow) related to a density increase. The dashed lines, respectively green for water and blue for glycerol, are the calculated form factor $F(Q)$ in bulk conditions.

The conclusions drawn here disagree with the results of Murata and Tanaka[5] who found, when temperature is rescaled by T_g, a smaller fraction of crystallized water for the fully hydrogenated sample from WAXS experiments. They estimate that the fraction of water that has crystallized is about 12% at 162 K ($T/T_g \approx 1.05$), 24% at 167 K ($T/T_g \approx 1.08$) and 34-44% at 170 K ($T/T_g \approx 1.10$). This is to be compared with what we find here: 21% for $T/T_g \approx 0.97$, 39% for $T/T_g \approx 1.03$, and 53% for $T/T_g \approx 1.09$. These lower estimates are possibly due to a less precise estimation procedure, an insufficient annealing time at the lowest temperatures, or an effectively slower cooling rate.

APPENDIX I: NEUTRON SPIN ECHO (NSE) RESULTS FOR THE DYNAMICS.

The typical neutron spin echo experiment consists in measuring the polarization at (so-called Fourier) times from $t = 0$ ps to 2000 ps. These values are then nor-

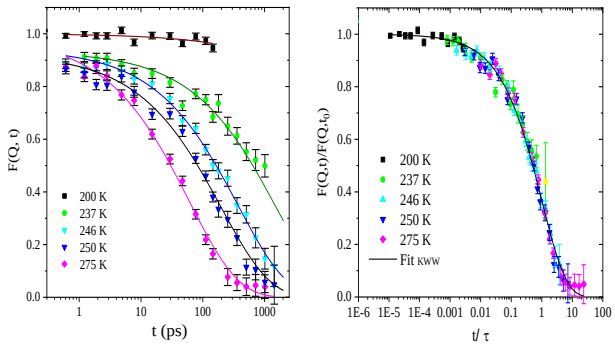

FIG. 15: Left: Normalized time-dependent coherent scattering function $F(Q,t)$ obtained by NSE at the wavevector Q of the maximum peak of the static structure factor, both in the stable and in the weakly supercooled liquid (which we refer to as liquid I): glycerol-water solution with $c_g = 0.178$. Right: Rescaling of the data by using time-temperature superposition; the full line is the best fit to a stretched exponential (KWW function).

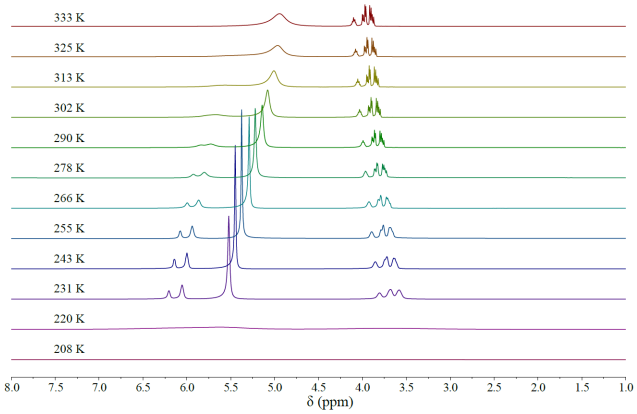

FIG. 16: Evolution of ^{1}H NMR spectra for the the glycerol/H_2O mixture ($c_g = 0.191$) as a function of temperature during the cooling stage.

malized by the signal at $t = 0$ and by the resolution function. Typical curves are shown in Fig. 15 (left) for $c_g = 0.178$ and for a range of temperatures in the stable and weakly supercooled liquid (200 to 280 K), which we refer to as liquid I, at the wavevector $Q = 1.9\mathring{A}^{-1}$ corresponding to the maximum of the structure factor in this range of temperature. A time-temperature superposition curve (right panel of Fig. 15) can then be built and fitted with a stretched exponential function (also known as Kohlrausch-Williams-Watts function) to obtain a more robust value of the stretching parameter $\beta_{\rm KWW}$: $f(t) = A\exp[-(t/\tau)^{\beta_{\rm KWW}}]$. The characteristic time τ is determined for each temperature to provide the best collapse on the master-curve. The stretching exponent is found to be $\beta_{\rm KWW} = 0.53$, a value comparable to that of other molecular glass-forming liquids in their supercooled regime. The experiments were performed on cooling and are reproducible in the temperature range studied.

We have similarly obtained the NSE data for the solutions with $c_g = 0.28$ and $c_g = 0.40$.

APPENDIX J: HIGH RESOLUTION ^{1}H NMR.

High resolution ^{1}H NMR allows one to give a clear complementary picture of the specific behavior of water and glycerol on a temperature range that covers the stable and the weakly supercooled liquid regime (liquid I). Fig. 16 presents the spectra of the glycerol/H_2O mixture ($c_g = 0.191$) as a function of temperature. At higher temperature, two set of peaks are observed, corresponding to the glycerol backbone (around 3.8 ppm) and to the mobile protons (around 5 ppm). This unique peak for the OH groups of glycerol and H_2O molecules is the signature of a rapid exchange regime between all these exchangeable hydrogen atoms. However, when the sample temperature is decrease below 313 K, this signal splits into two components, corresponding respectively to the OH groups of glycerol (above 6 ppm) and water (around 5.5 ppm). This results from a slowdown of the exchange regime between the groups belonging to glycerol and water. At even lower temperature (280 K), the two types of OH group of glycerol are also clearly split, which means an even longer residence time of all types of OH's on the glycerol molecules. Going to even lower temperatures, the signal broadens, indicating a strong decrease of molecular mobility. This phenomenon is reversible when heating the sample, with however a temperature hysteresis of around 20 K. In this domain, peak integration shows that half of the signal of water is lost compared to higher temperature, while the signal of glycerol is not affected. This is due to the selective crystallization of a fraction of the water in this mixture below 240 K. Further information can be gained from the measurement of the self-diffusion coefficients by pulsed-field gradient NMR. The specific behavior of each hydrogen group can be selectively measured. The variation of the self-diffusion coefficients with temperature is presented in Fig. 17: one can see that the ratio of the diffusion coefficient of water over that of glycerol increases from 2.7 at 295 K to 6 at 250 K. At high temperature, the self-diffusion coefficients of all the OH groups have similar values, significantly higher than that of the glycerol backbone. Note finally that the ratio between water and glycerol diffusion coefficients at 295 K is comparable to the value of 2.5 found for a fully deuterated sample at 298 K[18].

Around 265 K, one can notice that a fraction of the OH groups has the same diffusion coefficient as the glycerol backbone, indicating their longer residence time on glycerol. This slowing-down of the exchange rate is also seen in Fig. 17 where the apparent diffusion coefficients are measured as a function of the diffusion time at two

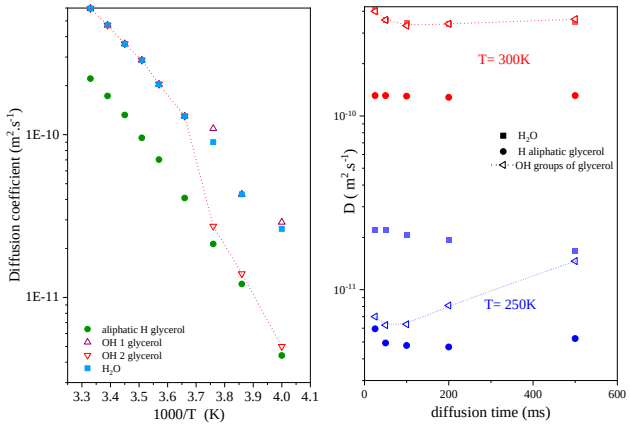

FIG. 17: (a) Evolution of the self-diffusion coefficients of the different hydrogen populations (aliphatic for the glycerol backbone, H_2O and the two populations of glycerol OH) for the glycerol/H_2O mixture ($c_g = 0.191$) as a function of temperature (measurements performed with a diffusion time of 100 ms). The ratio of the diffusion coefficient of water over that of glycerol increases from 2.7 at 295 K to 6 at 250 K. (b) Evolution of the apparent diffusion coefficients with the diffusion time, as measured at 250 K and 300 K.

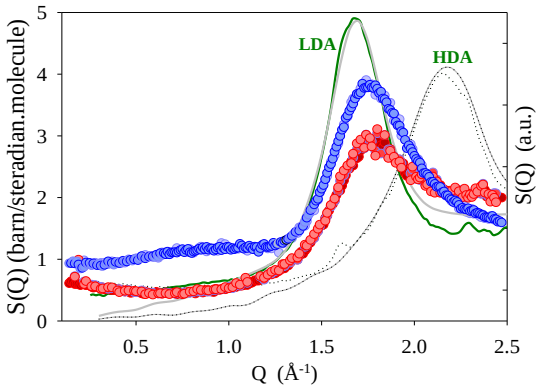

FIG. 18: Comparison between the static structure factor $S(Q)$ of liquid I' obtained by neutron scattering at 130, 160 and 170 K (blue symbols: $C_3H_5(OD)_3 + D_2O$; red symbols: $C_3D_5(OD)_3 + D_2O$) and that of the HDA at 77 K and the LDA at 120 K and 127 K (right axis, in arbitrary units; data from [15,16]).

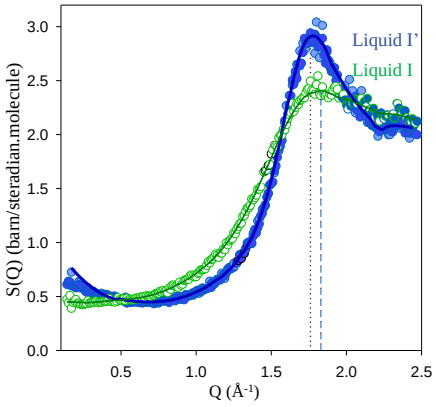

FIG. 19: Structure factor $S(Q)$ of liquid I at 260 K above melting (green symbols) and of glass/liquid I' at 130 K and 160 K (blue symbols) for the $c_g = 0.178$ glycerol-water solution. This illustrates the increased nano-segregation effect during cooling.

different temperatures. At high temperature, no variations are measured for diffusion time between 20 ms and 500 ms, indicating a Fickian-like behavior. However, at 250 K, the apparent diffusion coefficient of hydroxyl groups is strongly dependent on the diffusion time. At shorter time it is similar to that of the glycerol backbone, while at longer time it is water-like. This characterizes an exchange regime in the range of hundred of ms. The timescale over which nano-segregation locally persists therefore strongly increases with decreasing temperature.

APPENDIX K: STRUCTURE OF LIQUIDS I AND I'.

First we show that water in the nano-segregated liquid I' bears no resemblance to its high-density amorphous form and rather look like the low-density form: This is unambiguously seen from Fig. 18.

We also provide additional neutron-scattering structural data illustrating the difference between what we refer to as liquid I and liquid I' for the glycerol-water solution with $c_g \approx 0.18$.

In Fig. 19 we display the structure factor $S(Q)$ of liquid I at 260 K above melting and of that of liquid/glass I' at 130-160 K (prior to water crystallization). The maximum shifts from 1.83$\AA^{-1}$ at 260 K to 1.75$\AA^{-1}$ at 130 K, a trend which is typical of bulk water (see Fig. 14), and one can see an intensity increase at lower Q's at 170 K. These features are indications of an increased nano-segregation of water during the fast cooling (and during the subsequent heating to the annealing temperature, prior to ice formation). Further support comes for the fact that while the main peak follows the trend of bulk water the average liquid density conforms to the behavior of a conventional molecular liquid and increases between the high-temperature liquid I and the low-temperature liquid I'[13].

Finally, we also show a comparison of the evolution of the structure between liquid I (above melting) and glass/liquid I' at $c_g \approx 0.18$ and at a higher glycerol concentration $c_g = 0.28$. Although a detailed comparison is difficult because of the change in the weighting of the partial structure factors between $c_g \approx 0.18$ and $c_g = 0.28$, one can notice that the position of the main peak of liquid I' is around 1.75$\AA^{-1}$ and does not seem to change much with concentration. The variation with temperature (*i.e.*, between liquid I and liquid I') of

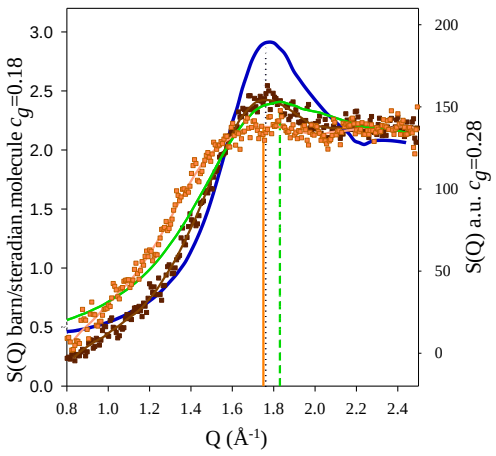

FIG. 20: Comparison of the structure factors of liquid I (green line) and liquid I' (blue line) for $c_g = 0.178$ (same data as in Fig. 19) with those of liquid I (orange squares and associated line) at 275 K and of glass/liquid I' at 130 K (brown squares and associated line) for a higher glycerol concentration $c_g = 0.28$.

the peak position is significant and goes to lower Q as T decreases for $c_g \approx 0.18$ whereas it is negligible for $c_g = 0.28$. The displacement to lower Q tracks the nano-segregation of water, and this effect disappears as c_g increases. We conjecture that at even higher glycerol concentration, for $c_g \gtrsim 0.38$, the peaks shifts to higher Q as T decreases, as seen in standard molecular liquids (see glycerol in Fig. 14).

* Electronic address: christiane.alba-simionesco@cea.fr
† Electronic address: tarjus@lptmc.jussieu.fr

[1] Broto, F. and Clausse, D. C., A study of the freezing of supercooled water dispersed within emulsions by differential scanning calorimetry. *J. Phys. C : Solid State Phys.* **9**, 4251-4257 (1976).
[2] K. Miyata and H. Kanno, Supercooling behavior of aqueous solutions of alcohols and saccharides. J. Molec. Liq. **119**, 189-193 (2005).
[3] Shen, C., Julius, E. F., Tyree, T. J., Moreau, D. W., Ataksi, H, and Thorne, R. E., Thermal Contraction of Aqueous Glycerol and Ethylene Glycol Solutions for Optimized Protein Crystal Cryoprotection. *Acta Cryst. D* **72**, 742-752 (2016).
[4] Lane, L. Freezing Points of Glycerol and its Aqueous Solutions. *Ind. Eng. Chem.* **17**, 924 (1925).
[5] Murata, K. and Tanaka, H. Liquid-liquid transition without macroscopic phase separation in a water-glycerol mixture. *Nature Materials* **11**, 436-443 (2012) and Supplementary Information.
[6] Inaba, A. and Andersson, O. Multiple glass transitions and two step crystallization for the binary system of water and glycerol. *Thermochimica Acta* **461**, 44-49 (2007).
[7] The larger temperature difference for the glass transition, which is 10-12 K for pure water and slowly decreases as c_g increases, stems from quantum effects observed at low temperatures: see Gainaru, C., Agapov, A. L., Fuentes-Landete, V., Amann-Winkel, K., Nelson, H., Köster, K. W., Kolesnikov, A. I., Novikov, V. N., Richert, R., Böhmer, R., Loerting, T., and Sokolov, A. P. Isotope effect in the glass transition of water, *PNAS* **111**, 17402-17407 (2014).
[8] Popov, I, Greenbaum Gutina, A., Sokolov, A. P., and Feldman, Y. The puzzling first-order phase transition in water-glycerol mixtures. *Phys. Chem. Chem. Phys.* **17**, 18063-18071 (2015).
[9] Nakagawa, H. and T. Oyama, T. Molecular Basis of Water Activity in Glycerol-Water Mixtures. Front. Chem. **7**, 731 (2019).
[10] Zhao, L.-S., Cao, Z.-X., and Q. Wang, Q. Glass transition of aqueous solutions involving annealing-induced ice recrystallization resolves liquid-liquid transition puzzle of water. *Sci. Rep.* **141**, 15714 (2015).
[11] Johari, G. P. Water's size-dependent freezing to cubic ice. *J. Chem. Phys.* **122**, 194504 (2005).
[12] Hansen,T. C., Koza, M. M., and Kuhs, W. F., Formation and annealing of cubic ice: I. Modelling of stacking faults. *J. Phys.: Condens. Matter* **20**, 285104 (2008); Hansen,T. C., Koza, M. M., Lindner, P., and Kuhs, W. F., Formation and annealing of cubic ice: II. Kinetic study. *J. Phys.: Condens. Matter* **20**, 285105 (2008).
[13] Shen, C., Julius, E. F., Tyree, T. J., Moreau, D. W., Ataksi, H, and Thorne, R. E. Thermal Contraction of Aqueous Glycerol and Ethylene Glycol Solutions for Optimized Protein Crystal Cryoprotection. *Acta Cryst. D* **72**, 742-752 (2016).
[14] Hayashi, Y., Puzenko, A., and Feldman, Y. Ice nanocrystals in glycerol-water mixtures. *J. Phys. Chem. B* **109**, 16979-16981 (2005).
[15] Koza, M. M., Schober, H., Fischer, H. E., Hansen, T., and Fujara, F. Kinetics of the high- to low-density amorphous water transition. *J. Phys.: Condens. Matter* **15**, 321-332 (2003).
[16] M.-C. Bellissent-Funel, Texeira, J, and Bosio, L. Structure of high-density amorphous water. II. Neutron scattering study. *J. Chem. Phys.* **87**, 2231-2235 (1987).
[17] Busselez, R., Lefort, R., Ghoufi, A., Beuneu, B., Frick, B., Affouard, F., and Morineau, D. The non-Gaussian dynamics of glycerol. *J. Phys.: Condens. Matter* **23**, 505102 (2011). Busselez, R. *Propriétés de fluides vitrifiables bio-*

protecteurs nanoconfinés. PhD Thesis #3802, University of Rennes 1, France (2008).

[18] D'Errico, G., Ortona, O., Capuano, F., and Vitagliano, V. Diffusion Coefficients for the Binary System Glycerol + Water at 25° C. *J. Chem. Eng. Data* **49**, 1665-1670 (2004).